

Review

Hafnia and hafnia-toughened ceramics

J. WANG

IRC in Materials for High Performance Applications, The University of Birmingham, Birmingham, B15 2TT

H. P. LI, R. STEVENS

School of Materials, The University of Leeds, Leeds LS2 9JT

Hafnia (HfO_2) and hafnium-based materials are traditionally regarded as technologically important materials in the nuclear industry, a consequence of their exceptionally high neutron absorption coefficient. Following the discovery of transformation toughening in the mid 1970s, a considerable research effort has been devoted to zirconia (ZrO_2)-toughened ceramics (ZTCs). They are considered to be potentially useful materials for structural applications at low and intermediate temperatures ($T < 1000^\circ\text{C}$). Their unsuitability for high-temperature structural applications ($T > 1000^\circ\text{C}$) is related to the low temperature of the tetragonal to monoclinic transformation in ZrO_2 . On the basis that HfO_2 exhibits a similar crystal structure and in particular that its tetragonal to monoclinic transformation temperature ($\sim 1700^\circ\text{C}$) is approximately 700°C higher than that for ZrO_2 , it has been suggested that high-temperature transformation toughening could be possible in HfO_2 -toughened ceramics (HTCs). Although the concepts behind this suggestion are universally appreciated, only a limited success has been made of the fabrication and the microstructural and mechanical property evaluation of these materials. The fracture toughness values obtained so far in HfO_2 toughened ceramics are, in fact, considerably lower than those obtained in their ZrO_2 counterparts. A great deal of further research work is therefore required in order to understand fully and to exploit toughened ceramics in the HfO_2 -based and HfO_2 -containing systems. This review covers the science and technology of HfO_2 and HfO_2 -toughened ceramics in terms of processing, phase transformation, microstructure, and mechanical properties.

1. Introduction

There has been a considerable progress in the science and technology of ZrO_2 and ZrO_2 -toughened ceramics (ZTCs) in the last decade, following the discovery of transformation toughening in the mid 1970s [1–5]. Such progress is best evinced by the considerable number of international conferences and published volumes devoted specifically to these materials.

The properties of these toughened ceramics are exceptional. A fracture toughness (K_{IC}) of $> 15 \text{ MPa m}^{0.5}$, which is almost comparable with that of cast iron, and a fracture strength of 2.4 GPa, have been measured for ZrO_2 -toughened ceramics [6–10]. However, the potentially important applications for these ZrO_2 -toughened ceramics are greatly reduced by their thermal instabilities both at low ($200\text{--}400^\circ\text{C}$) and at high ($T > 1000^\circ\text{C}$) temperatures [11, 12]. It is theoretically impossible to retain transformation toughening in these ceramics at temperatures above 1000°C , as the tetragonal ZrO_2 phase becomes thermodynamically stable at temperatures above its monoclinic to tetragonal transformation temperature [13, 14]. In view of the fact that HfO_2 has a very similar structure to ZrO_2 , and more importantly, that it has a higher

tetragonal to monoclinic transformation temperature ($\sim 1700^\circ\text{C}$) than ZrO_2 , HfO_2 and HfO_2 -toughened ceramics have been widely discussed as potential substitutes for ZrO_2 and ZrO_2 -toughened ceramics at elevated temperatures [15–18], Fig. 1. They are expected to exhibit toughening mechanisms such as stress-induced transformation and compressive surface stress at temperatures up to $\sim 1700^\circ\text{C}$. Accordingly, such suggestions have stimulated considerable interest and some research effort into HfO_2 and HfO_2 -toughened ceramics in the last few years, although a considerably great effort will be required to make significant progress [19].

Hafnium-based materials, on the other hand, are traditionally regarded as a class of valuable materials in nuclear industries, as they have an exceptionally high neutron cross-section absorption coefficient ($> 150 \text{ cm}^2/\text{atom} \times 10^{24}$ for thermal neutrons) [20–22]. Their high neutron absorption coefficients, for example, make them attractive as a control rod material in water-cooled reactors. Zirconium-based materials, in contrast, have an extremely low specific neutron cross-section absorption coefficient ($< 0.5 \text{ cm}^2/\text{atom} \times 10^{24}$ for thermal neutrons) such that

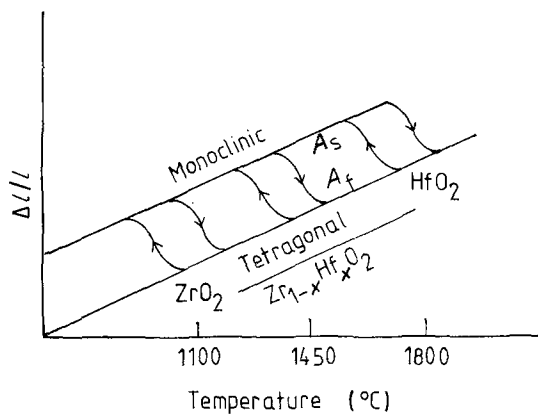


Figure 1 The influence of HfO_2 alloying on the monoclinic \rightleftharpoons tetragonal transformation temperature in ZrO_2 - HfO_2 . A_s and A_f refer to the monoclinic to tetragonal starting and finishing temperatures, respectively. It is expected that high-temperature transformation toughening can be achieved when ZrO_2 is fully or partially substituted by HfO_2 [17].

they are a useful cladding material for nuclear fuels [23, 24]. HfO_2 ceramics, known to have a melting point of 2800°C , are also very useful as a high temperature refractory material [15].

The first comprehensive review on HfO_2 ceramics was made by Lynch [15], who summarized the early research work on these materials some twenty years ago, in terms of crystal structure, properties and fabrication. Naturally, this review is outdated when one considers the recent development in the science and technology of HfO_2 and HfO_2 -toughened ceramics made especially in the last decade. Transformation toughening was unrecognized until the mid 1970s [2, 3, 25]. The class of transformation-toughened ceramics containing HfO_2 are therefore more appreciated as a structural material than was previously the case. It is the aim of this review to present a summary of the recent development in HfO_2 and HfO_2 -toughened ceramics with respect to their applications as structural materials. As they are similar to ZrO_2 and ZrO_2 -toughened ceramics in many respects, a comparison is regularly made between these two classes of materials in the present review. Consequently, certain results for ZrO_2 and ZrO_2 -toughened ceramics are included in this review.

2. Origin of the similarity between HfO_2 and ZrO_2 : lanthanide contraction

Until the discovery of hafnium by Coster and Hevesey in 1923 and the summary by Hevesey [26] in 1925, the original determination of the atomic weight of zirconium (first discovered in 1789) was generally too high, due to the unrecognized presence of hafnium. Hafnium compounds are remarkably similar to those of zirconium both in structure and in chemistry [27, 28]. For example, the structures of HfO_2 and ZrO_2 are so close to each other that it is difficult to detect their individual presence using conventional powder X-ray diffraction [29]. The formation of a continuous solid solution in the HfO_2 - ZrO_2 system has long been confirmed [30]. Both the self- and inter-diffusion coefficients of hafnium and zirconium are similar in value,

as observed by Sakka *et al.*, [31] in ZrO_2 -16 mol % CaO and $\text{Zr}_{1-x}\text{Hf}_x\text{O}_2$ -16 mol % CaO ceramics.

The great similarity between hafnium compounds and those of zirconium, such as exists between HfO_2 and ZrO_2 , is related to the electron configurations of hafnium and zirconium: (i) $4f^{14}5d^26s^2$ for hafnium, and (ii) $4d^25s^2$ for zirconium. In the periodic table, the inner transition (rare-earth) elements immediately preceding hafnium add electrons to the inner 4f shell from cerium through to lutetium. Because no outer electrons have been added to compensate for the increased nuclear charge, there is a contraction in the atomic size such that element 72, hafnium, has a slightly smaller atomic size than element 40, zirconium, the preceding period group IV element. This results in the so-called lanthanide contraction. The atomic radii of hafnium and zirconium are close to each other [32]: 0.1442 and 0.1454 nm, respectively. So are their ionic radii (M^{4+}), 0.084 nm for hafnium and 0.083 nm for zirconium, respectively [32, 33]. The electronegativity values given by Little and Jones [34] are 1.23 for hafnium and 1.22 for zirconium. These values are indicative of the almost identical chemistries exhibited by hafnium and zirconium [35] and explain the origin of the similarity between HfO_2 and ZrO_2 .

3. Occurrence and processing

3.1. Occurrence

Hafnium, which has an estimated abundance of 4.5 p.p.m. in the Earth's crust [36], is always found in nature accompanying zirconium. The principal commercial sources for hafnium are baddeleyite (a naturally occurring hafnium-containing zirconia mineral, $\text{Zr}(\text{Hf})\text{O}_2$), and zircon (hafnium-containing zirconium silicate, $\text{Zr}(\text{Hf})\text{SiO}_4$), which are best known as the prime mineral sources for ZrO_2 . World production of these minerals in 1984 was 700 000 tonnes, 451 000 tonnes of which were produced in Australia, 93 000 tonnes in the USA and 144 000 tonnes in South Africa [37, 38]. These naturally occurring minerals typically contain 1.5–3 wt % hafnium, with respect to the zirconium content [39]. Most of the commercially available zirconium compounds (such as ZrO_2 powders used in the ceramic industry) contain this level of hafnium content as an expected and understood impurity [40, 41]. However, certain engineering applications, such as those in the nuclear industry, require both high-purity hafnium and high-purity zirconium products for specific purposes [42–46]. Current production of hafnium is thus entirely dependent on the availability of zirconium compounds as a by-product. Consequently, hafnium compounds are much more expensive than those of zirconium. For example, \$600/kg HfO_2 is compared with \$50/kg ZrO_2 [40, 41, 47–49]. The high cost of hafnium compounds is, to a large extent, due to the difficulties involved in their separation from those of zirconium.

3.2. Processing of HfO_2 -based ceramics

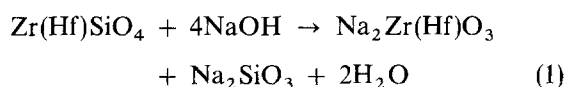
The processing of HfO_2 -based ceramics often starts with hafnium and hafnium compounds (such as

hafnium tetrachloride), which are originally separated from the hafnium-containing zirconia-based minerals. The nuclear industry is the principal sector involved in the extraction of hafnium from the naturally occurring zirconia minerals. The extraction process essentially involves two stages: (i) the processing of hafnium-containing zirconium compounds (such as oxide, chloride, nitrate, acetate) from zircon and baddeleyite [50–52]; and (ii) the subsequent separation of hafnium from these zirconium compounds [52–54].

3.2.1. The processing of hafnium-containing zirconium compounds

The techniques for this are essentially those utilized for obtaining zirconium compounds from the naturally occurring minerals. They start with mining of zircon ores or baddeleyite, followed by the removal of undesirable elements, such as silica, which is the major impurity constituent in zircon. Several techniques can be utilized to extract hafnium-containing zirconium compounds from zircon, including alkali oxide decomposition, chlorination, thermal decomposition, lime fusion, and plasma dissociation. In the following, a brief is given of the alkali oxide decomposition and chlorination, as they are the most widely employed extraction processes in industry.

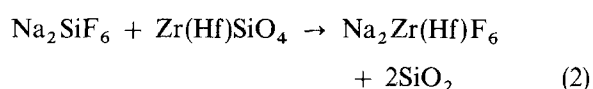
3.2.1.1. Alkali oxide decomposition. This processing technique is widely used for obtaining zirconia-based materials from zircon. At temperatures above 600 °C, zircon and sodium hydroxide (NaOH) react to form sodium zirconate, $\text{Na}_2\text{Zr}(\text{Hf})\text{O}_3$, and sodium silicate, Na_2SiO_3 . Careful control of the reaction conditions, such as the zircon/sodium hydroxide ratio, temperature, and time, will lead to a complete conversion according to the reaction



In industry, sodium hydroxide is often substituted by sodium carbonate. The reaction then requires a higher temperature (~ 1000 °C) than when sodium hydroxide is used and the resultant products are also dependent on conditions such as the zircon/sodium carbonate ratio and reaction temperature.

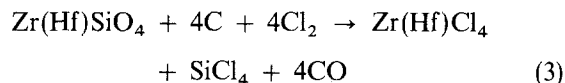
After the above conversion, sodium silicate can be subsequently removed from the products by leaching with water, which at the same time hydrolyses sodium zirconate to form zirconium hydroxide. The hydroxide is usually converted into chloride for extracting hafnium from zirconium. Zirconium hydroxide can also be directly calcined to give a low-purity ZrO_2 for conventional ceramic applications. Further purification processes, such as leaching with sulphuric acid, will generate a high-purity product.

For the specific extraction of hafnium from zircon (this will be discussed in Section 3.2.2), $\text{Na}_2\text{Zr}(\text{Hf})\text{F}_6$ is produced by reacting zircon with sodium silicofluorite (Na_2SiF_6) according to



This reaction is carried out by firing the reaction mixture in a kiln at temperatures in the region of ~ 700 °C for an appropriate period.

3.2.1.2. Chlorination. The direct chlorination process is particularly useful in extracting hafnium from zircon. In the presence of carbon, zircon can be directly chlorinated



An intimate mixing of zircon and carbon, usually achieved by milling and pelletizing, will enhance the completion of the above reaction. For large-scale productions, the above reaction is usually carried out at 800–1200 °C in a shaft furnace or a fluidized bed. Hafnium-containing zirconium tetrachloride ($\text{Zr}(\text{Hf})\text{Cl}_4$) and silicon tetrachloride (SiCl_4) are distilled off from the furnace and then condensed at 165 °C and -10 °C, respectively, resulting in the separation of the former from the latter. As will be discussed in the following section, HfCl_4 can be extracted out from $\text{Zr}(\text{Hf})\text{Cl}_4$ using the differential solvent extraction technique [23, 55]. Hafnium metal (almost all the hafnium now produced) is made by reducing hafnium tetrachloride with magnesium or with sodium [32]. Alternatively, hafnium can be extracted out from hafnium-containing zirconium oxychloride, $\text{Zr}(\text{Hf})\text{OCl}_2$, which is a hydrolysed product of $\text{Zr}(\text{Hf})\text{Cl}_4$, using the fractional crystallization technique [54, 56].

Hafnium oxychloride is commercially available both in an aqueous solution and in powder form. The hafnium oxychloride powder is made by cooling a saturated HfOCl_2 solution from 65 °C to 20 °C in rubber-lined tanks, then followed by drying at 85 °C. As will be discussed later, a wide range of finely divided HfO_2 powders, which are usually sinterable at relatively low temperatures (~ 1500 °C), can be made from HfOCl_2 or HfCl_4 via a precipitation route. For example, hafnium hydroxide is precipitated out from a HfOCl_2 solution by an ammonia solution at pH of 10–11, and the subsequent calcination at 500–600 °C will convert the hydroxide into the desired oxide powder. Partially and fully stabilized HfO_2 powders, such as Y_2O_3 -doped HfO_2 powders, are made in a similar way, where $\text{Y}(\text{NO}_3)_3$ or YCl_3 solution is mixed with the HfOCl_2 solution.

3.2.2. Separation

The separation and purification processes for hafnium from zirconium compounds are costly and tedious, a consequence of the considerable similarity of their chemical characteristics. Only the nuclear industry is interested in such separation and purification techniques for obtaining high-purity (no more than a few p.p.m. zirconium) hafnium-based materials for specific applications and have therefore pursued the development of these techniques over the last four decades. Small differences in certain physical and chemical

properties, such as in solubility, absorption, electro-negativity, vapour pressure, and boiling temperature, between hafnium compounds and zirconium compounds are made use of for the separation and purification processes. More than a dozen techniques have been developed and can be used to extract hafnium from hafnium-containing zirconium compounds. These include:

(i) fractional crystallization of hafnium and zirconium hexafluorides, oxychlorides, and oxalates [54];

(ii) fractional precipitation of hafnium and zirconium phosphates and ethyl phosphates [57];

(iii) fractional distillation of POCl_3 addition compounds of $\text{Zr}(\text{Hf})\text{Cl}_4$ [58];

(iv) fractional decomposition of hafnium and zirconium complex compounds [59];

(v) differential solvent extraction [23, 55];

(vi) ion-exchange technique [60];

(vii) differential deposition [21, 22];

(viii) differential displacement [24, 56, 61], involving the oxidation-reduction equilibria of zirconium and hafnium between a molten salt phase and a molten zinc phase.

Amongst these various separation techniques, the organic solvent extraction is probably the most widely used method [23, 55, 61]. This technique makes use of the solubility difference in certain organic solvents between ZrCl_4 and HfCl_4 . As discussed earlier, zircon can be directly chlorinated at temperatures of around 1000°C , resulting in the formation of a corresponding mixture of ZrCl_4 and HfCl_4 (the mixture was written as $\text{Zr}(\text{Hf})\text{Cl}_4$ earlier). This product mixture is then mixed with water and ammonium thiocyanate and passed through a liquid-liquid counter-current separation column containing organic solvents such as methyl isobutyl ketone (MIBK). If each column is considered to be a separation stage, a separation factor of 5 can be achieved after each stage. Therefore, a sufficiently long separation column or enough separation columns will lead to a significantly high separation factor. The separated HfCl_4 is converted into either hafnium metal for the nuclear applications or hafnium oxide (HfO_2) for the ceramic applications.

As mentioned previously, zircon reacts with sodium (or potassium) silico-fluorite at $\sim 700^\circ\text{C}$ to form a mixture of Na_2ZrF_6 and Na_2HfF_6 (the mixture was written as $\text{Na}_2\text{Zr}(\text{Hf})\text{F}_6$ earlier). The mixture is dissolved in water in which the hafnium salt is about twice as soluble as the zirconium salt. This operation is then repeated through a large number of stages until the desired separation of the hafnium salt from the zirconium salt is achieved.

In the differential deposition technique [21, 22], the vapour mixture of zirconium tetrachloride and hafnium tetrachloride are passed over zirconium metal. Zirconium trichloride, which has a higher deposition tendency on the surface of zirconium metal than hafnium tetrachloride, is separated from the undeposited hafnium tetrachloride vapour. A separation factor as high as 10 can be made in each operation. Zirconium tetrachloride is recovered by heating and disproportionation. Similarly, the mixture of zirconium tetrachloride and hafnium tetrachloride can be dis-

tilled off at an appropriate pressure and temperature [58], resulting in the separation of hafnium from zirconium. However, the low separation factor (~ 2 per operation) of this technique limits its application for the large-scale production.

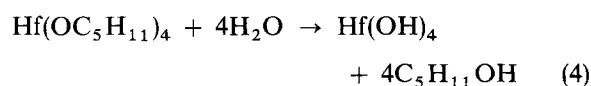
Recently, a US patent [61] described a separation process, which makes use of the fact that hafnium is slightly more electropositive than zirconium [34]. A molten metal solution of unseparated zirconium and hafnium is kept in contact with a fused metal solvent phase which contains cations more electropositive than zirconium. The solvent phase also contains zirconium ions (such as sodium fluoro-zirconate). Hafnium is transported from the molten metal phase to the fused salt phase while zirconium is transported from the fused salt phase to the molten metal phase. The separation efficiency is dependent on the type of the solvent phase. For example, a separation factor of 10 can be achieved when the molten phase of zirconium-hafnium metal is kept in contact with a molten sodium fluoro-zirconate. A significantly high separation factor, up to 300, is possible in a single separation step, when zinc, cadmium, lead, bismuth, copper or tin are used as the solvent metals.

3.2.3. Preparation of HfO_2 powders

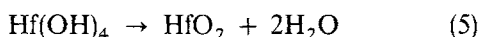
The fabrication of HfO_2 -based and HfO_2 -containing ceramics usually starts with the manufacture of high-purity and sinterable HfO_2 powders which, unfortunately, are expensive and not widely available commercially. The powder compacts are then densified, using means such as conventional sintering, hot pressing (HPing), and hot isostatic pressing (HIPing). The starting materials for powder preparation in laboratory scale are the commercially available hafnium chemicals, such as hafnium alkoxide, nitrite, oxynitrite, chloride, and oxychloride. High-purity hafnium metal, which is largely used in the nuclear industry, also appears to be useful in preparing fine HfO_2 powders. As HfO_2 is such a similar material to ZrO_2 , it is easy to appreciate that the powder preparation routes developed for ZrO_2 ceramics are equally applicable to HfO_2 ceramics. The following is a brief survey of the powder preparation routes which were specifically developed for HfO_2 ceramics.

3.2.3.1. Alkoxy method. Hafnium alkoxides, such as $\text{Hf}(\text{OC}_3\text{H}_7)_4$, $\text{Hf}(\text{OC}_4\text{H}_9)_4$ and $\text{Hf}(\text{OC}_5\text{H}_{11})_4$, were used by Mazdidasni *et al.* [62, 63] to prepare high-purity HfO_2 powders (particle size 5–20 nm, and purity $> 99.995\%$) via either vapour-phase decomposition or hydrolytic decomposition. These authors [64, 65] also prepared Y_2O_3 -stabilized HfO_2 powders using the same technique, where an appropriate amount of yttrium alkoxide was mixed together with hafnium alkoxide.

For the hydrolytic decomposition, hafnium hydroxide was obtained by slowly adding deionized triply distilled water to a spectrograde tetrakis tertiary amyl-oxide of hafnium



The hydroxide was then dried in vacuum at 50 °C for 24 h



3.2.3.2. Precipitation method. Dole *et al.* [66] developed a precipitation technique using hafnium nitrite, oxynitrite and hydrochloride as the starting materials, to prepare highly sinterable HfO₂ powder. The same technique was used to prepare partially and fully stabilized HfO₂ ceramics [67]. Alternatively, hafnium metal can be used. As was demonstrated by Tau *et al.* [68] and by Srinivasan and Davis [69], hafnium-containing nitric acid solution can be obtained by first dissolving a high-purity hafnium metal (> 99.9%) in a hydrofluoric acid and followed by repeated precipitation dissolutions using ammonia solution and nitric acid. Hafnium hydroxide is precipitated out by slowly adding ammonia solution into the hafnium-containing acid solution. This is followed by:

- (i) water wash to remove ammonia salts;
- (ii) an initial acetone wash to convert the water medium into organic medium;
- (iii) toluene wash to strip off water; and finally
- (iv) acetone wash again to remove toluene.

The resultant material will become a friable powder at room temperature within 30 min. HfO₂ powders can also be obtained by directly calcining the precipitated hafnium hydroxides at 500 °C for 2 h.

3.2.3.3. Hydrothermal oxidation method. The hydrothermal oxidation technique was largely employed by Toraya *et al.* [70–74] for preparing monolithic HfO₂, doped HfO₂ and mixed Al₂O₃ + HfO₂ powders. For monolithic HfO₂, hafnium metal powders (particle size 15 μm) and redistilled water (2:1 H₂O/Hf mole ratio) were sealed by electric arc welding into a platinum capsule (2.7 mm inner diameter). The hydrothermal oxidation was carried out at temperatures of 300–700 °C and at pressures of 80–150 MPa for 3–60 h. For mixed Al₂O₃ + HfO₂ powders, HfAl₃ alloy (or mixed hafnium and aluminium metal powders) and redistilled water was sealed into a platinum capsule, followed by a similar hydrothermal treatment. The resultant powder, which exhibited a very fine crystallite size (20–50 nm) and narrow size distribution, was highly sinterable.

In their study on the martensitic transformation in small-sized HfO₂ and ZrO₂ powders, Chen and Chiao [75, 76] used an internal oxidation technique to prepare their samples which had particle sizes of 50–100 nm.

4. Structure and phase transformation

Table I is a summary of the lattice parameters describing the structures of HfO₂. The corresponding values for ZrO₂ are also included in Table I for comparison. In several instances, earlier values, such as those reported in 1950s by Curtis *et al.* [80], are omitted in the literature in favour of later values. Two apparent observations can be made from Table I:

(i) the tabulated values obtained by different investigators are in a good agreement; and

(ii) HfO₂ and ZrO₂ exhibit close similarity in their crystal structure.

4.1. Crystal structure

The well established classical studies on the crystal structure of ZrO₂ by numerous investigators can serve as a guide to explain the crystal structure of HfO₂ [86, 88–92].

4.1.1. Monoclinic HfO₂

The crystal structure of monoclinic HfO₂ was first accurately determined by Adam and Rogers [77], whose results are contained in Table I. The results are so similar to those of ZrO₂ that the general descriptions for monoclinic ZrO₂ given by McCullough and Trueblood [89] and Smith and Newkirk [90], and recently summarized by Subbarao [12], can equally apply to monoclinic HfO₂:

(i) seven-fold coordination of Zr(Hf)⁴⁺ with a range of bond lengths and bond angles, Fig. 2;

(ii) layers of triangularly coordinated O_I-Zr(Hf)³⁺ and tetrahedrally coordinated O_{II}-Zr(Hf)⁴⁺ (slightly distorted), Fig. 3;

(iii) Zr(Hf)⁴⁺ ions are located in layers parallel to the (100) planes, separated by O_I and O_{II} atoms on either side; and

(iv) the layer thickness is wider when the Zr(Hf)⁴⁺ ions are separated by O_I atoms than when they are separated by O_{II} atoms.

On the other hand, a slight difference exists in the dimension of their unit cells, although they demonstrate such an almost identical monoclinic structure [77, 79, 93]. In general, the unit cell of monoclinic HfO₂ is slightly smaller than that of monoclinic ZrO₂. This difference is theoretically predictable and is consistent with the ionic radii of Hf⁴⁺ and Zr⁴⁺, which were given as 0.083 and 0.084 nm, respectively [32, 33].

A further detailed study on the structural parameters of monoclinic HfO₂ single crystals (needle-like), which were grown from a lithium molybdate melt, was made by Ruh and Corfield [93]. Using Weissenberg techniques, they worked out the coordination positions of Hf⁴⁺ and O²⁻ ions. A similar study was recently carried out on polycrystalline HfO₂ powder by Hann *et al.* [79], who obtained the structural parameters using powder X-ray diffraction. Tables II and III show the atomic coordinates and interatomic distances in monoclinic HfO₂ and ZrO₂ obtained by these authors. It is seen that the results obtained by these two groups are in good agreement. The interatomic distances are slightly smaller in monoclinic HfO₂ than in monoclinic ZrO₂. For example, the average Hf–O_I and Hf–O_{II} distances (0.2086 and 0.2197 nm, respectively) are slightly smaller than the corresponding Zr–O_I and Zr–O_{II} distances (0.2090 and 0.2211 nm, respectively). The average Hf–Hf distances in the O_{Ic} and O_{IIa} coordination polyhedra (0.3547 and 0.3386 nm, respectively) are

TABLE I A survey of the structural parameters for HfO₂ and ZrO₂

	<i>a</i> (nm)	<i>b</i> (nm)	<i>c</i> (nm)	β (deg)	Space group	Reference
Mono. HfO ₂	0.51156	0.51722	0.52948	99.18	P2 ₁ /c	[77]
	0.5119	0.5169	0.5290	99.25		[30]
	0.5117	0.5172	0.5284	99.37		[78]
	0.5117	0.51754	0.52915	99.22		[79]
	0.5110	0.514	0.528	99.70		[80]
	0.511	0.517	0.528	99.60		[81]
	0.5112	0.5171	0.5286	99.20		[82]
	0.512	0.518	0.525			[29]
	0.497	0.524	0.518			[83]
	0.5106	0.5148	0.5273	99.33		[65]
Mono. ZrO ₂	0.5156	0.5191	0.5304	98.9	P2 ₁ /c	[38]
	0.5145	0.5208	0.5311	99.23		[79]
Tetr. HfO ₂	0.514		0.525		P4 ₂ /nmc	[80]
	0.515		0.5295 (1760 °C)			[82]
	0.5155		0.5285			[81]
	0.5175		0.5325 (2000 °C)			[84]
Tetr. ZrO ₂	0.5094		0.5177		P4 ₂ /nmc	[38]
Cubic HfO ₂	0.5110 (1600 °C)				F _{3m3}	[85]
	0.508					[83]
	0.53 (2750 °C)					[84]
	0.5144					[86]
	0.51155					[66]
	0.5122					[87]
Cubic ZrO ₂	0.5124				F _{3m3}	[38]
	0.5256 (2300 °C)					[82]

TABLE II The atomic coordinates in monoclinic HfO₂ and ZrO₂

	Atom coordinates in HfO ₂			Reference	Atom coordinates in ZrO ₂			Reference
	Hf	O _I	O _{II}		Zr	O _I	O _{II}	
<i>x</i>	0.2759	0.0730	0.446	[93]	0.2758	0.069	0.451	[89]
	0.2755	0.0739	0.4489	[79] ^a	0.2758	0.0703	0.4423	[90]
	0.2755	0.0742	0.4487	[79] ^b	0.2742	0.0630	0.4491	[79] ^a
					0.2742	0.0628	0.4485	[79] ^b
<i>y</i>	0.0412	0.346	0.748	[93]	0.0404	0.342	0.758	[89]
	0.0397	0.3318	0.7582	[79] ^a	0.0411	0.3359	0.7549	[90]
	0.0397	0.3316	0.7581	[79] ^b	0.0389	0.3289	0.7548	[79] ^a
					0.0389	0.3279	0.7554	[79] ^b
<i>z</i>	0.2078	0.332	0.488	[93]	0.2089	0.345	0.479	[89]
	0.2078	0.3466	0.4800	[79] ^a	0.2082	0.3406	0.4789	[90]
	0.2080	0.3467	0.4801	[79] ^b	0.2095	0.3476	0.4827	[79] ^a
					0.2095	0.3471	0.4819	[79] ^b
<i>B</i> (10 ² nm ²)	0.45	0.45	0.45	[93]	1.0	1.4	1.4	[89]
	0.0	0.0	0.0	[79] ^a	0.303	0.317	0.317	[90]
	0.05	0.4	0.8	[79] ^b	0.0	0.0	0.0	[79] ^a
					0.15	1.01	1.01	[79] ^b
<i>N</i>	1.0	1.0	1.0	[93]	1.0	1.0	1.0	[89]
	1.04	1.06	1.0	[93] ^a	1.0	1.0	1.0	[90]
	0.99	1.03	1.0	[93] ^b	0.98	1.07	1.0	[79] ^a
					0.91	1.04	1.0	[79] ^b

^a Values calculated with isotropic temperature factor.

^b Values calculated with individual temperature factor.

also smaller than the corresponding Zr–Zr distances (0.3565 and 0.3406 nm, respectively). The O_{IIa}–O_{IIb} distance differs the most, 0.262 and 0.272 nm for HfO₂ and ZrO₂ respectively, although even this seemingly large difference is not significant because these ions are related by a symmetry centre. Because of the reduced interatomic lengths, the array of O_{II} atoms in mono-

clinic HfO₂ more closely approaches a square array than in monoclinic ZrO₂.

4.1.2. Tetragonal HfO₂

As in the case of the monoclinic form, tetragonal HfO₂ is also almost identical to the tetragonal form of ZrO₂,

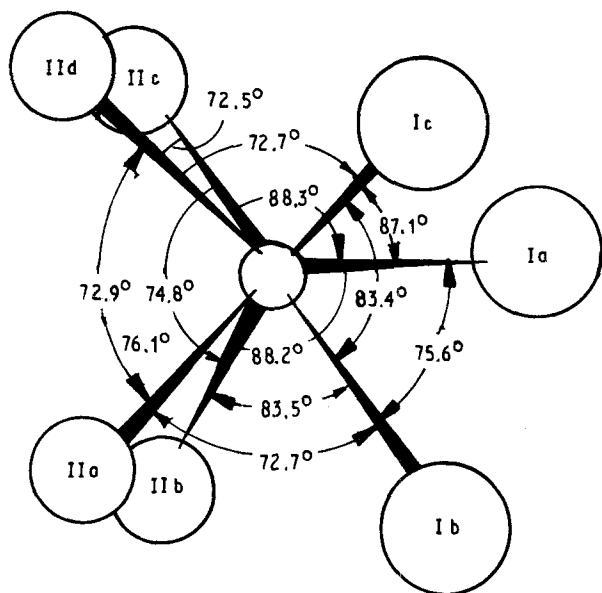


Figure 2 The orientation and angles of the oxygen atoms in the ZrO_7 coordination polyhedron in ZrO_2 , showing the seven-fold coordination of the Zr^{4+} ion. HfO_2 has a very similar structure [89, 90].

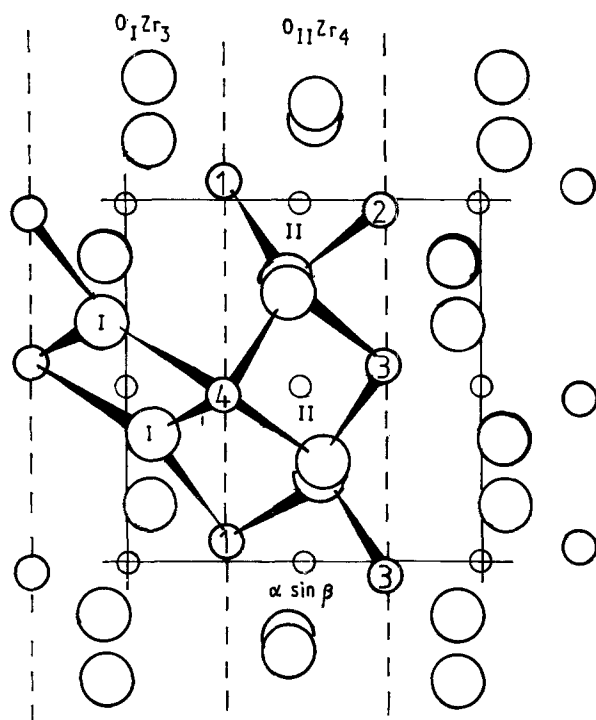


Figure 3 The projection of the crystal structure of monoclinic ZrO_2 along the C_m -axis showing layers of $O_I Zr_3$ and $O_{II} Zr_4$ polyhedron [89, 90].

which can be regarded as a distorted fluorite-type cubic structure [80, 81, 94, 95]. Teufer [91] showed that Zr^{4+} was surrounded by eight O^{2-} ions, four at a distance of 0.2455 nm and the other four at a distance of 0.2065 nm.

The tetragonal phase in HfO_2 was first detected by Curtis *et al.* [80], using high-temperature X-ray diffraction at temperatures from 1640–1920 °C. Its lattice parameters and the tetragonal to monoclinic transformation temperature have since been studied by a number of investigators [81, 95–97]. As is indicated in

TABLE III The interatomic distances (nm) in monoclinic HfO_2 and ZrO_2 [93]

(a) M–O distances in the $M(3)$ coordination polyhedron

O	Hf–O distance	Zr–O distance
Ia	0.2031	0.2057
Ib	0.2174	0.2163
Ic	0.2052	0.2051
IIa	0.2170	0.2189
IIb	0.2162	0.2220
IIc	0.2202	0.2151
IId	0.2254	0.2285

(b) O–O distances in the $M(3)$ coordination polyhedron

O	O	HfO_2	ZrO_2
Ia	Ib	0.259	0.259
Ia	Ic	0.279	0.283
Ib	Ic	0.283	0.280
IIa	IIb	0.262	0.272
IIb	IId	0.265	0.266
IIb	IIc	0.265	0.266
IIc	IId	0.267	0.262

(c) M–M distances in the O_{Ic} coordination polyhedron

M	M	HfO_2	ZrO_2
1	2	0.3318	0.3334
1	3	0.3906	0.3329
2	3	0.3417	0.3433

(d) M–M distances in the O_{IId} coordination polyhedron

M	M	HfO_2	ZrO_2
1	2	0.3449	0.3469
1	3	0.3438	0.3460
1	4	0.4010	0.4031
2	3	0.3417	0.3433
2	4	0.3438	0.3460
3	4	0.3571	0.3580

Table I, the unit cell of tetragonal HfO_2 is slightly larger than that of tetragonal ZrO_2 . It can therefore be concluded that the Hf–O bond length is slightly larger than the Zr–O bond length in the tetragonal phase. This is the reverse of the case for the monoclinic symmetry, as described earlier.

4.1.3. Cubic HfO_2

The cubic HfO_2 phase has a fluorite-type structure, in which each Hf^{4+} ion is coordinated by eight equidistant O^{2-} ions and each O^{2-} ion is tetrahedrally coordinated by four Hf^{4+} ions [98].

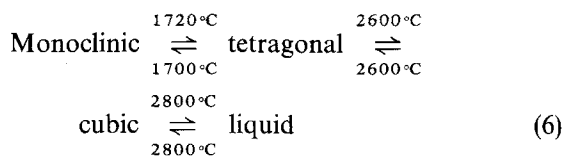
Only a limited number of structural studies exist in published literature for cubic HfO_2 . The values suggested for its lattice parameter are contained in Table I [83, 86, 92, 95].

4.2. Phase transformations

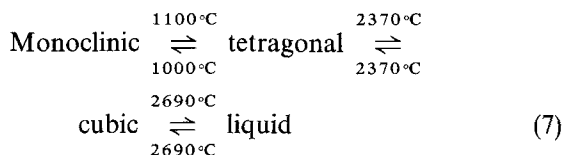
Both temperature and pressure affect the polymorphism of HfO_2 . This section presents its phase transformations as a function of temperature at atmospheric pressure. The orthorhombic HfO_2 phase,

which can be preserved at an appropriate combination of pressure and temperature [99], is discussed in Section 6.1.

HfO₂ exhibits the following transformations with increasing temperature [100, 101].



Similarly, ZrO₂ exhibits [102, 103]



It is seen that HfO₂ follows the same transformation sequence as ZrO₂ with a noticeable increase in each transformation temperature of the monoclinic \rightleftharpoons tetragonal \rightleftharpoons cubic \rightleftharpoons liquid. Among these transformations, the tetragonal to monoclinic has been that most extensively studied and has the most important technological implication in terms of transformation toughening for structural ceramics. The less technologically important tetragonal to cubic transformation has not been studied in detail, possibly as a consequence of the experimental difficulties experienced in working at high temperatures ($\sim 2600^{\circ}\text{C}$). As will be discussed below, the monoclinic \rightleftharpoons tetragonal transformations start and complete at different temperatures. The exact temperatures at which each transformation starts and completes are not well agreed by different authors. Thus, the temperature values indicated above are for guidance purposes only.

4.3. Tetragonal to monoclinic transformation

Wolten [101] was the first to suggest that the tetragonal to monoclinic transformation was martensitic in nature. A well-framed picture has now been built up, after extensive investigations into this martensitic transformation during the last three decades. The following brief summary of the results obtained by various investigators for the tetragonal to monoclinic transformation, commonly applied both to HfO₂ and to ZrO₂ [94] can be given.

(i) The high-temperature tetragonal phase cannot be quenched to room temperature.

(ii) There is an abrupt change in the lattice parameters at the transformation [100, 101, 104–106], Fig. 4a and b. It is shown that HfO₂ and ZrO₂ are strongly anisotropic in thermal expansion, with the *b*-axis exhibiting negligible expansion while the expansion is substantial for the *a*- and *c*-axes.

(iii) The phase transition is athermal, as established by XRD, metallographic study, and DTA. Thus, it does not take place at a fixed temperature but over a temperature range, i.e. the amount of the transformed phase varies with change in temperature but not as a function of time at a particular temperature, Fig. 5.

(iv) The transformation exhibits a large thermal hysteresis, i.e. the heating and cooling transformations

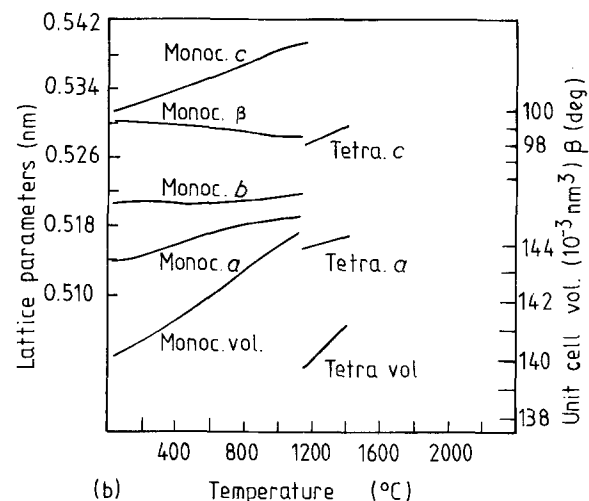
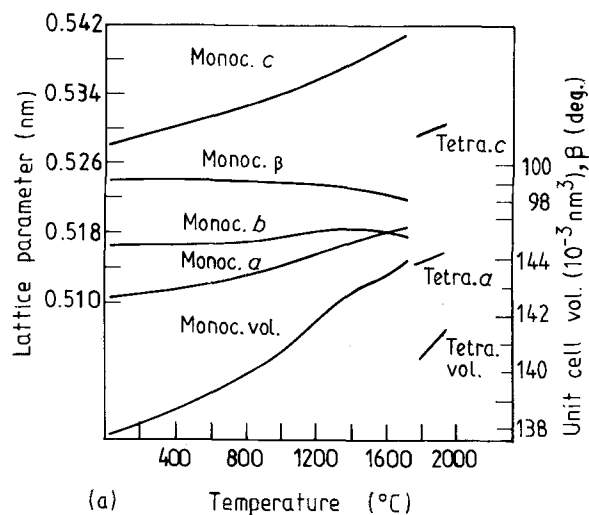


Figure 4 The thermal expansion behaviour of (a) HfO₂ and (b) ZrO₂, showing that there is a volume contraction at the monoclinic to tetragonal transformation temperature, and that their axial expansions are highly anisotropic [100, 105].

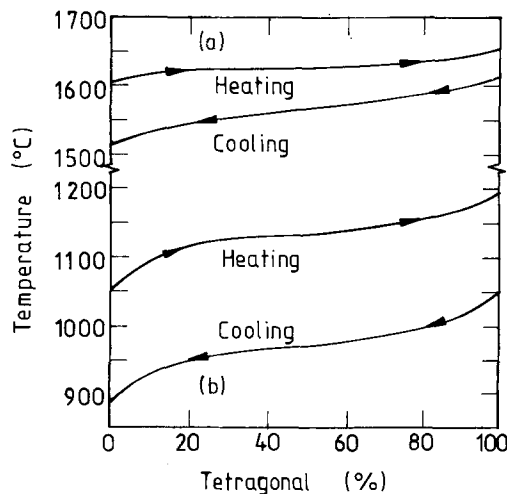


Figure 5 The monoclinic \rightleftharpoons tetragonal transformations in (a) HfO₂ and (b) ZrO₂, determined by high-temperature X-ray diffraction. The hysteresis effect is smaller in HfO₂ than in ZrO₂ [93]. The monoclinic \rightleftharpoons tetragonal transformation temperatures indicated for HfO₂ in this diagram are slightly below the average values agreed by most other investigators.

TABLE IV A summary of the reported transformation temperatures in HfO₂ and ZrO₂

	Monoclinic to tetragonal	Tetragonal to monoclinic	Reference
	Starting (completion) (°C)	Starting (completion) (°C)	
HfO ₂	1540 (1650)	1590 (1510)	[101]
	1610 (1655)	1625 (1515)	[93]
	1620 (1650)	1620 (1520)	[30]
	1725		[82]
		1700	[87]
		1740	[109]
		1750	[81]
		1793	[85]
	1800		[110, 111]
	1830		[112]
ZrO ₂	1050 (1110)	910 (804)	[101]
	1160 (1215)	1038 (993)	[30]
Tetragonal ⇌ cubic (°C)			
HfO ₂	2520		[30]
	2530		[113]
	2660		[109]
	2700		[15, 78]
ZrO ₂	2370		[7, 38]
Cubic ⇌ liquid (°C)			
HfO ₂	2753		[114]
	2774		[115]
	2800		[113, 116]
	2803		[117]
	2810		[118]
	2820		[112, 119, 120]
	2870		[109]
	2900		[15, 78, 80]
ZrO ₂	2680		[7, 38]

starting and finishing at different temperatures [100, 101], Fig. 5.

(v) The transformation is associated with a volume expansion, a shear strain and microtwinning [104–106].

(vi) The transformation is a diffusionless process, in which the atoms retain their neighbours in either phase. O²⁻ ions undergo an atomic movement of less than one interatomic distance and Zr(Hf)⁴⁺ ions a minor shift.

(vii) There is an established orientation relationship between the parent and product phases. The transformation exhibits habit planes and lattice invariant deformations.

(viii) There is a critical grain size for the transformation, below which the tetragonal phase can be retained at temperatures less than the transformation temperature, and above which the spontaneous tetragonal to monoclinic transformation occurs on cooling from sintering temperature. This critical grain size phenomenon has been considered to be a surface energy effect [107, 108].

4.4. Characteristics of the tetragonal to monoclinic transformation in HfO₂

Although HfO₂ has a remarkably similar structure and phase transformation to ZrO₂, its tetragonal to

monoclinic transformation has several characteristics which effectively make it different from ZrO₂ for transformation toughening.

(i) The tetragonal to monoclinic transformation temperature (~1700 °C) is several hundred degrees higher than that for ZrO₂ (~1000 °C), Table IV.

(ii) The difference between the heating transformation (monoclinic to tetragonal) temperature and the cooling transformation (tetragonal to monoclinic) temperature is smaller than that which occurs in ZrO₂, i.e. the temperature hysteresis effect in HfO₂ is less pronounced than that in ZrO₂. Fig. 5 shows that the temperature hysteresis loops for HfO₂ and ZrO₂ have a similar shape but differ in widths (40–80 °C for HfO₂, and 150–200 °C for ZrO₂) [93].

(iii) The established density change (2.5% to 3.4%) [121] associated with the transformation in HfO₂ is much smaller than is found in ZrO₂ (5% to 7.5%) [80, 96]. This implies that the volume expansion and shear strain associated with the transformation in the former are smaller than those in the latter.

(iv) Under strain-free conditions, the critical grain size for retaining the tetragonal phase in HfO₂ (4–10 nm) [122] at room temperature is much smaller than that in ZrO₂, (15–30 nm) [75, 76, 123, 124]. It is therefore considerably more difficult to retain the metastable tetragonal HfO₂ phase than it is to retain tetragonal ZrO₂ in a ceramic matrix in terms of the critical grain-size effect.

4.5. Theories of the tetragonal to monoclinic transformation

It is acceptable that the theories which have been proposed to account for the tetragonal to monoclinic transformation in ZrO_2 are equally applicable to HfO_2 . There is general agreement that the transformation event involves both nucleation and subsequent growth processes and that the phase transformation itself is nucleation controlled [75, 76, 125, 126]. However, there is a strong disagreement as to how the nucleation is induced, although the difference could well have arisen due to the different materials employed for different approaches. Two well-known conflicting theories which are used to interpret the nucleation of the martensitic transformation are the “non-classical” model supported by Ruhle and Heuer [125, 126] and the “classical” model proposed by Chen and Chaio [75, 76]. The “non-classical” model involves a continuous sequence of states along the reaction path, i.e. there is a locally continuous distortion of the parent phase into the martensitic product in small but finite regions, until a critically sized nucleus of the product phase is reached. Therefore the nucleation is a homogeneous process. On the basis of thermodynamic data and *in situ* microstructural observation (TEM), Ruhle and Heuer [125, 126] suggested that the nucleation was invariably stress-assisted, the stress arising from microstructural defects, thermal expansion mismatch or morphology effects.

In contrast, the “classical” model suggested by Chen and Chaio [74, 75] proposes that the nucleation is a heterogeneous process, the formation of the martensitic nucleus being a sudden event. Thermodynamically, it is assisted by the stresses associated with microstructural defects, such as microcracks, lattice defects or the areas where the concentration of alloying oxide is below the average value. These authors demonstrated a clear relationship between the particle size and the possibility of nucleating the martensitic transformation. Recently, Wang *et al.* [127] observed a direct relationship between the mechanical properties (fracture strength and fracture toughness) and grain size in Y_2O_3 -stabilized tetragonal zirconia polycrystalline (Y-TZP) ceramics. It was suggested that the high transformability of the large grain sized Y-TZP ceramics was related to the increased amount of martensitic nuclei available.

As discussed above, although HfO_2 and ZrO_2 exhibit almost identical crystal structures and the isovalent hafnium and zirconium have nearly equal ionic radii [32, 33], the tetragonal to monoclinic transformation temperature in the former is several hundred degrees higher than in the latter. This phenomenon is surprising when one views their great structural similarity.

Two explanations have been suggested to account for such a surprising discrepancy. Grain and Campbell [104] proposed a critical metal–oxygen bond length (M–O) model to account for the increased monoclinic to tetragonal transformation temperature in HfO_2 with respect to that in ZrO_2 . It is believed that this model is valid to explain the tetragonal to monoclinic transformation temperature in HfO_2 . On

the other hand, Garvie and Chan [128, 129] worked out a partially soft lattice mechanism to interpret the high tetragonal to monoclinic transformation temperature in HfO_2 .

The critical M–O length model, suggested by Grain and Campbell [104], is based on the idea that the monoclinic phase will transform into tetragonal phase when the M–O bond length approaches a critical value, with increasing temperature. To appreciate this model, it will be helpful to look at the temperature dependence of the lattice parameters for HfO_2 and ZrO_2 , as shown in Fig. 4a and b. The lattice parameters at a particular temperature are dependent both on the values at room temperature and the average thermal expansion coefficients. As was shown in Table I, the unit cell of monoclinic HfO_2 is slightly smaller than that of monoclinic ZrO_2 at room temperature. The average thermal expansion coefficient of the former is also below that of the latter (this will be discussed in Section 8.1). At $\sim 1050^\circ C$, where monoclinic ZrO_2 starts to transform into tetragonal ZrO_2 , the unit cell of monoclinic HfO_2 is essentially smaller than that of ZrO_2 . Because the unit cell dimension is directly related to the M–O bond length, the Zr–O bond length is therefore larger than the Hf–O bond length at $1050^\circ C$.

If the Zr–O bond length is considered to be the critical variable for the monoclinic to tetragonal transformation, such that the monoclinic structure is no longer stable when the M–O bond length reaches the critical value, then the Hf–O bond length at $1050^\circ C$ is apparently below this critical value. This suggestion can be indirectly supported by the fact that if the lattice parameters for HfO_2 are extrapolated from $1050^\circ C$ to $1720^\circ C$ on the basis of thermal expansion coefficient, they will become very close to those of monoclinic ZrO_2 at $1050^\circ C$. $1720^\circ C$ is, in fact, approximately the monoclinic to tetragonal transformation temperature for HfO_2 . Specifically, the Hf–O bond length will not reach the critical M–O bond length for the monoclinic to tetragonal transformation until $1720^\circ C$ is approached. This view is also consistent with the fact that both HfO_2 and ZrO_2 can be stabilized by other alloying oxides, such as Y_2O_3 , MgO, CaO and oxides of most rare-earths, or via the creation of oxygen vacancies. In these stabilized materials, the dimension of the unit cell is effectively reduced because of the oxygen loss, thus making the M–O distance shorter than it would be in the stoichiometric form.

The partially soft lattice mechanism, proposed by Garvie and Chan [128, 129] to account for the increased tetragonal \rightarrow monoclinic transformation temperature in HfO_2 , is based on the fact that the atomic mass of hafnium (178.49) is much greater than that of zirconium (91.22), although they have almost identical atomic radii and electronegativity [32–34]. These authors derived a direct relationship between the atomic mass and the transformation temperature in the tetragonal structure and then applied the relationship to ZrO_2 and to HfO_2 – ZrO_2 solid solution, respectively. According to this mechanism [128, 129], the tetragonal to monoclinic transformation temperature in the

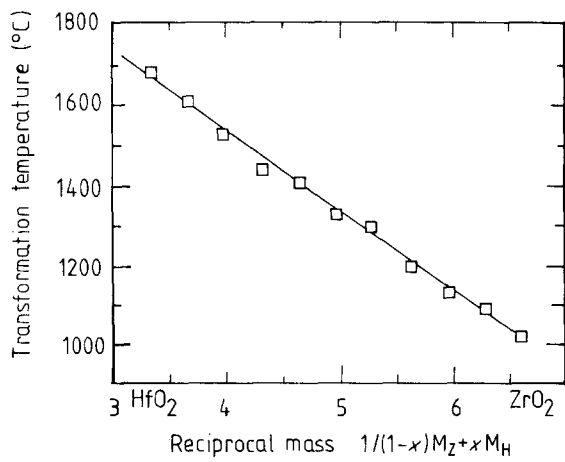


Figure 6 The experimental plot of the tetragonal to monoclinic transformation temperature in ZrO_2 - HfO_2 solid solution as a function of the reciprocal effective mass [128, 129]. These results agree well with the prediction of the partially soft lattice mechanism.

HfO_2 - ZrO_2 solid solution, T_{HZ} , may be written as

$$T_{HZ} = -k/\{\bar{\beta}[(1-x)M_Z + xM_H]\} + \Delta \quad (8)$$

where k is a combination of force constants, $\bar{\beta}$ is a positive constant, x is the mole fraction of HfO_2 and M_Z and M_H the masses of zirconium and hafnium, respectively. Δ is a parameter determined by the elastic constants of the solid solution.

It is seen that the tetragonal to monoclinic transformation temperature increases with increasing HfO_2 alloying in ZrO_2 . This theoretical consideration agrees well with the experimental results, Fig. 6, which is a plot of the experimental values of T_{HZ} versus $1/[(1-x)M_Z + xM_H]$. The transformation temperatures for pure HfO_2 and ZrO_2 are worked out to be 1680 and 1030 °C when assuming x is 1 and 0, respectively. This is in good agreement with the experimental results obtained by other investigators.

5. The retention of metastable tetragonal HfO_2 phase

The mechanical properties (both the fracture toughness and the fracture strength) of transformation-toughened ceramics are affected by several parameters associated with the tetragonal to monoclinic transformation. According to Evans and co-worker [130-132], the toughness increment due to the stress-induced martensitic transformation in ZrO_2 -toughened ceramics may be expressed as

$$K_c = \eta E e^T V_f h^{0.5} / (1 - \nu) \quad (9)$$

in which E is the Young's modulus of the system, ν is Poisson's ratio, e^T is the effective volume expansion associated with the transformation, h the transformation zone width, V_f the volume fraction of tetragonal phase susceptible to transformation at crack tip, and η is a constant determined by the nature of the transformation.

If it is assumed that the above equation is equally applicable to HfO_2 -toughened ceramics, it can thus be appreciated that the fracture toughness increment associated with the tetragonal to monoclinic trans-

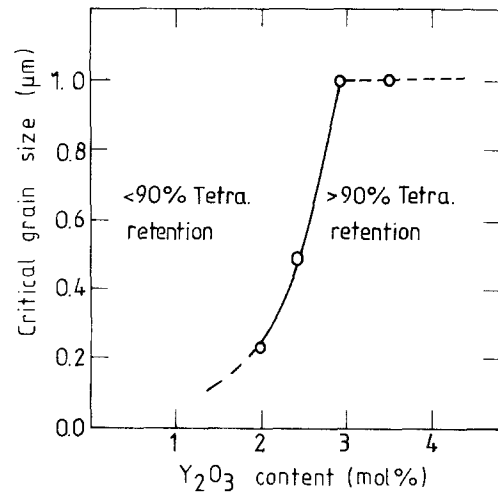


Figure 7 The critical grain size for spontaneous tetragonal to monoclinic transformation as a function of Y_2O_3 content in ZrO_2 [133].

formation of HfO_2 will be determined by the amount of transformable tetragonal phase retained in the matrix, the transformation zone size, and the effective volume expansion associated with the transformation. It is therefore desirable to retain a high volume fraction of highly transformable tetragonal phase in order to obtain a significantly improved fracture toughness. In ZrO_2 -based ceramics, there have been established a few structural and composition parameters which have been proved to influence the retention of the metastable tetragonal phase, including grain size, grain morphology, type and amount of stabilizers, and the matrix constraint [133-135]. A relationship between the transformability and these parameters are well established after extensive research work in the last decade. Both the type and the amount of stabilizers have a strong influence on the critical grain size for retaining tetragonal ZrO_2 phase. Fig. 7 shows the critical grain size as a function of Y_2O_3 content for Y_2O_3 -doped ZrO_2 ceramics, illustrating a sharp increase in the critical grain size in the range of 2-3 mol % Y_2O_3 [133]. In sintered ceramic matrices, tetragonal inclusions of 2-3 μm can be retained for Y_2O_3 (2-3 mol %)-stabilized ZrO_2 [127].

The grain-size effect in HfO_2 -toughened ceramics has not been studied to the same extent when compared to that of their ZrO_2 counterparts. Only a very limited amount of experimental work has been done to measure the critical grain size for retaining the metastable tetragonal phase in either doped or undoped HfO_2 [67, 122, 123]. In theory, the same thermodynamic analysis procedures as those for ZrO_2 [123, 136] can be made pertaining to the conditions for retaining the metastable tetragonal phase in HfO_2 . Amongst many thermodynamic studies which have been made for ZrO_2 -based systems, those by Bailey *et al.* [123, 124] and by Lange [136] are widely accepted. For simplicity, the present authors prefer the one made by Bailey *et al.* [123, 124].

At temperatures below the tetragonal to monoclinic transformation temperature, a tetragonal HfO_2 particle is metastable when its size is small enough, i.e. below a critical value, as the tetragonal phase has a

lower surface energy than the monoclinic phase [107, 108]. A spontaneous tetragonal to monoclinic transformation needs to satisfy the following thermodynamic expression

$$(G_T - G_M) + (S_T\gamma_T - S_M\gamma_M) + (V_T - V_M) = 0 \quad (10)$$

where the expression takes account of the volume free energy change ($G_T - G_M$), the surface energy change ($S_T\gamma_T - S_M\gamma_M$), and the strain energy change ($V_T - V_M$), of the transformation. The following equation can be further developed

$$D_c = 6(\gamma_M/\rho_M - \gamma_T/\rho_T)/[(G_T - G_M) + (V_T - V_M)] \quad (11)$$

in which D_c is the critical grain size for spontaneous tetragonal to monoclinic transformation, γ_M and γ_T are the specific surface energies and ρ_M and ρ_T are densities for monoclinic and tetragonal phases, respectively.

A value of $10.46 \text{ kJ mol}^{-1}$ was used by Schick [137] for the volume energy change term. A value of 2.7% was given by Stacy [121] for the effective volume increase associated with the tetragonal to monoclinic transformation in HfO_2 . Values for all the other terms in the equation can be taken from those for ZrO_2 , as was done by Whitney [138, 220]. The resulting value for the critical grain size to undergo the spontaneous tetragonal to monoclinic transformation in HfO_2 is $\sim 4 \text{ nm}$. This value is in a reasonably good agreement with experimental results obtained by Hunter *et al.* [122], who observed that the critical grain size was $\sim 10 \text{ nm}$ for pure HfO_2 under strain-free conditions. It is therefore to be concluded that the critical grain size for retaining metastable tetragonal HfO_2 phase is in the range of 4–10 nm.

One will readily realize the difficulties in retaining tetragonal HfO_2 inclusions of 4–10 nm in a sintered ceramic matrix via conventional fabrication techniques. Such difficulties are well supported by the fact that the retention of a high volume fraction of tetragonal HfO_2 phase (e.g. $> 50\%$) has never been reported in either an HfO_2 -based system or in HfO_2 -toughened ceramics [67]. As an example, 46% was the highest volume fraction of metastable tetragonal HfO_2 phase retained, in Er_2O_3 -doped HfO_2 ceramics which were fabricated using a hot-pressing technique [67, 122]. As was found by Tau *et al.* [68], it was almost impossible to retain any tetragonal phase in the HfO_2 powders chemically prepared using a precipitation technique, a process which has been recognized and would lead to a fine particle size. The situation was completely different in the ZrO_2 powders, in which a high percentage of tetragonal phase (up to 100%) could be retained when the pH value of the supernatant liquid used to form the powders lay within certain ranges (from 2–4 and from 12–14). Tau *et al.* [68] further observed that, in an appropriate pH range, the amount of tetragonal phase retained in the coprecipitated HfO_2 - ZrO_2 powders decreased rapidly with increasing HfO_2 content. Unfortunately, these authors were unable to correlate their phase analysis results

to the particle sizes of these chemically prepared powders.

As suggested by Evans and co-worker [130–132], another vitally important parameter in determining the toughness increment induced by the transformation toughening is e^T , the effective strain energy term associated with the volume expansion and shear strain of the transformation. The volume expansion in HfO_2 was measured to be lower than that in ZrO_2 [15, 30, 93], although the exact value has not been agreed by different authors. The axial and volume thermal expansion curves illustrated in Fig. 4a and b, for example, clearly show that the volume expansion associated with the tetragonal to monoclinic transformation in HfO_2 is smaller than that in ZrO_2 . The value worked out by Ruh *et al.* [30, 93] was 2.7% for HfO_2 , compared with 5%–7.5% for ZrO_2 [15]. In their study of transformation toughening in the Al_2O_3 - Cr_2O_3 / ZrO_2 - HfO_2 system, Brog and co-workers [139, 140] observed that the density of microcracks induced by the tetragonal to monoclinic transformation decreased with increasing HfO_2 alloying in the HfO_2 - ZrO_2 solid solution. These authors believed that the reduced microcrack density was due to the reduced volume expansion associated with HfO_2 alloying in ZrO_2 . Therefore, it is considered disadvantageous to utilize HfO_2 as a toughening agent in terms of its small volume expansion and the shear strain associated with the tetragonal to monoclinic transformation.

6. HfO_2 based systems

6.1. High-pressure orthorhombic HfO_2

The existence of a high-pressure orthorhombic phase in HfO_2 has been observed by several investigators [141–145] although there exists considerable disagreement as to the pressure at which the orthorhombic structure could be preserved. The first notable experiment on the P - T diagram (the pressure-temperature diagram) for HfO_2 was due to Bocquillon *et al.* [141]. According to these authors, the orthorhombic polymorph could be preserved at pressures of $> 2 \text{ GPa}$ at ambient temperature, as shown in Fig. 8. The orthorhombic phase transforms to the monoclinic phase on prolonged heating at 300°C at atmospheric pressure. Therefore, the monoclinic to orthorhombic transformation is reversible.

Two recent studies on the high-pressure polymorphs in HfO_2 and ZrO_2 and their solid solutions were due to Liu [99] and Suyama *et al.* [146]. Liu noted at least two very interesting phenomena, which were in disagreement with the results obtained by Bocquillon *et al.* [141], namely the pressure at which the monoclinic phase transforms to the orthorhombic phase and the transformation sequence at temperatures below 1200°C . Monoclinic HfO_2 was found to transform to orthorhombic HfO_2 at pressures greater than 15 GPa (ZrO_2 had the same transformation at 10 GPa). This value is therefore considerably different from the value in Fig. 8. At 1200°C or below, with increasing pressure the transformation follows the sequence of monoclinic (baddeleyite) \rightarrow tetragonal \rightarrow

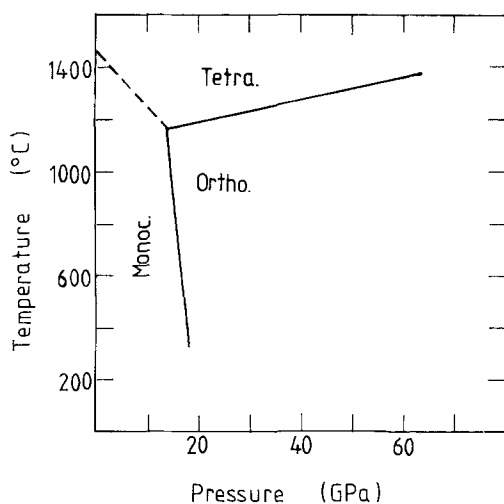


Figure 8 The P - T diagram established by Bocquillon *et al.* [141] for HfO_2 . (---) The monoclinic-tetragonal boundary proposed by these authors, not observed experimentally. The results shown in this diagram are very much different from those of Liu [99] and Suyama *et al.* [146].

orthorhombic (cotunnite-type), with the polyhedral co-ordination varying from 7, 8 to 9. This again differs from the results in Fig. 8, which shows that at temperatures below 1200 °C, the transformation follows the sequence of monoclinic \rightarrow orthorhombic, with increasing pressure. Unfortunately, Liu [99] failed to present a P - T diagram for HfO_2 , although he worked out such a diagram for ZrO_2 . However, he pointed out that HfO_2 should exhibit a similar diagram to that for ZrO_2 , except where all the polymorphs occur at relatively higher pressures and temperatures in comparison with those of ZrO_2 .

Liu [99] also believed that the orthorhombic HfO_2 and ZrO_2 phases he preserved at 15 GPa and at 1000 °C exhibited a cotunnite-type structure. Therefore, the lattice parameters of orthorhombic HfO_2 and ZrO_2 worked out by him are significantly different from those by Suyama *et al.* [146], Table V.

Suyama *et al.* [146] preserved the orthorhombic HfO_2 - ZrO_2 solid solutions at a pressure of 6 GPa and at 600 °C in a cubic anvil device. Although they worked out their lattice parameters, as a function of composition, they omitted to present a P - T diagram for the HfO_2 - ZrO_2 system. Table VI and Fig. 9 show that the unit cell dimensions of the orthorhombic HfO_2 - ZrO_2 solid solution decrease linearly toward those of HfO_2 . This is due to the reduced unit cell of orthorhombic HfO_2 in comparison with that of orthorhombic ZrO_2 .

6.2. Stabilization

Adding another alloying oxide in ZrO_2 to form a solid solution is the most commonly used method to modify the tetragonal to monoclinic transition temperature [1, 6, 7]. The stabilization of cubic and tetragonal ZrO_2 phases by means of solid solution formation with the alloying oxides has been widely investigated over the last decade, following the discovery of transformation toughening in the mid 1970s [1]. It is essential to form and to retain the metastable tetragonal phase in sintered ceramic bodies for improving

TABLE V The lattice parameters obtained by Liu [99] and Suyama *et al.* [146] for the orthorhombic HfO_2 and ZrO_2

Materials	Lattice parameters (nm)			Reference
	a	b	c	
HfO_2	0.3311	0.5550	0.6461	[99]
	0.5007	0.5055	0.5224	[146]
ZrO_2	0.3328	0.5565	0.6503	[99]
	0.5044	0.5089	0.5259	[146]

TABLE VI The lattice parameters of orthorhombic HfO_2 - ZrO_2 solid solutions ($\text{Hf}_{1-x}\text{Zr}_x\text{O}_2$) [146]

Compositions (x)	Lattice parameters (nm)		
	a	b	c
0.00	0.5007	0.5055	0.5224
0.26	0.5016	0.5063	0.5236
0.50	0.5024	0.5071	0.5243
0.74	0.5035	0.5083	0.5249
1.00	0.5044	0.5089	0.5259

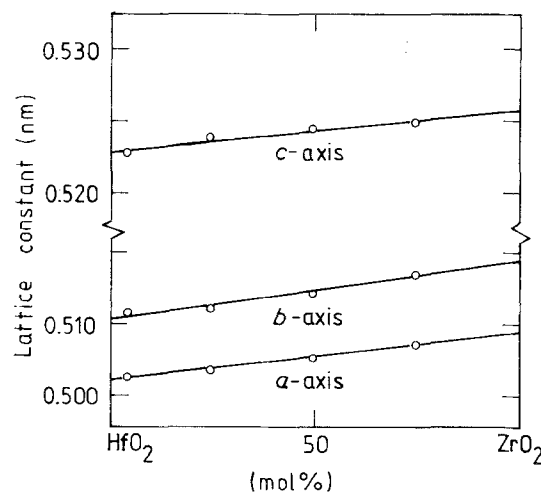


Figure 9 The lattice parameters as a function of composition for the orthorhombic HfO_2 - ZrO_2 solid solution [146], illustrating an almost linear decrease towards HfO_2 .

mechanical properties. The alloying oxides used include Y_2O_3 , MgO , CaO , CeO_2 and oxides of most rare-earths. In particular, the microstructure and mechanical properties have been extensively exploited in the Y_2O_3 - MgO - and CeO_2 - ZrO_2 systems [147]. Highly toughened tetragonal zirconia polycrystals (TZPs) are obtainable in the Y_2O_3 - and CeO_2 -doped ZrO_2 ceramics, via a careful composition and processing control. Because HfO_2 is so similar to ZrO_2 in structure and phase transformation, it has been considered that such results may be equally plausible for HfO_2 .

When HfO_2 is alloyed with an alloying oxide, it may form a monoclinic (M_{ss}), tetragonal (T_{ss}) or a cubic solid solution (F_{ss}), ordered compounds, depending on the composition and individual system. In general, the oxide of an alkaline-earth element (MO) may form with HfO_2 the following types of compounds [84, 148]: $\text{MHf}_5\text{O}_{11}$, MHf_4O_9 , $\text{M}_2\text{Hf}_7\text{O}_{16}$,

$M_6Hf_{19}O_{44}$, $MHfO_3$, M_2HfO_4 , $M_3Hf_2O_7$ and $M_4Hf_3O_{10}$. For example, compounds $CaHfO_3$, $CaHf_4O_9$, $Ca_2Hf_7O_{16}$, and $Ca_6Hf_{19}O_{44}$ form in the HfO_2 -CaO system [13, 149]. The oxide of a rare-earth element and its analogue (M_2O_3) may form with HfO_2 the following types of compounds [148]: $M_2Hf_7O_{17}$, $M_2Hf_5O_{13}$, $M_2Hf_2O_7$, $M_4Hf_3O_{12}$, $M_5Hf_2O_{11.5}$ and M_6HfO_{11} . There probably exists the greatest number of compounds in the HfO_2 - Sc_2O_3 system. The oxide of an element with smaller cationic radius than hafnium forms with HfO_2 large regions of solid solutions. In contrast, no such large regions of solid solutions form in the case of that with larger cationic radius than hafnium.

6.3. Phase relationships in some important HfO_2 -based systems

6.3.1. The HfO_2 -Hf system

The phase relationships in the HfO_2 -Hf system was earlier studied independently by Rudy and Stecher [150] and Domagala and Ruh [151]. Both investigations involved metallographic analysis, X-ray diffraction, and hardness and melting point studies. These early studies showed that a continuous oxygen deficiency occurred in monoclinic and tetragonal HfO_2 with decreasing oxygen content. To a certain extent, HfO_2 was stabilized via an occurrence of oxygen deficiency in structure, e.g. both the cubic to tetragonal and the tetragonal to monoclinic inversion temperatures were lowered in oxygen-deficient HfO_2 . This phenomenon was similar to that in the ZrO_2 -Zr system [152]. Although the results obtained were in such general agreement, one region of disagreement was the $HfO_2/HfO_2 + \alpha$ -Hf phase boundary. Rudy and Stecher [150] found this boundary at 63.5 at % O, whereas Domagala and Ruh [151] obtained a value of 66 at % O.

A recent investigation into this system was due to Ruh and Patel [78], who proposed a diagram shown in Fig. 10 for the HfO_2 -rich portion. According to this diagram, a slight oxygen deficiency in HfO_2 results in

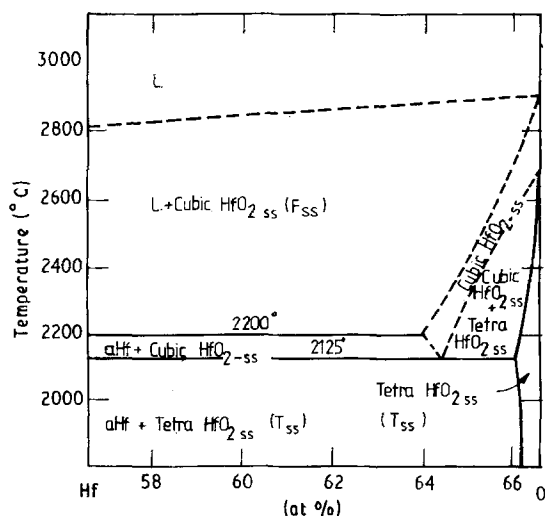


Figure 10 The phase diagram for the Hf-O(HfO_2) system, proposed by Ruh and Patel [78].

a dramatic reduction in the temperature for the cubic to tetragonal transformation. The cubic HfO_2 solid solution (F_{ss}) and α -Hf two-phase region exists in the temperature range 2150–2200 °C. When the cubic HfO_2 solid solution is quenched, it transforms to tetragonal HfO_2 solid solution (T_{ss}), with a sharp change in the solubility of α -Hf in HfO_2 , resulting in the formation of a striated precipitate of α -Hf at grain boundaries. The oxygen-deficient or non-stoichiometric HfO_2 was, however, shown to exhibit similar lattice parameters as those of stoichiometric HfO_2 .

6.3.2. The HfO_2 -CaO system

A phase diagram for the HfO_2 -CaO system was first proposed by Delamarre and Perez Y Jorba [153]. They observed the formation of cubic solid solution (F_{ss}) in the compositions containing > 10 mol % CaO at temperatures above 1450 °C, and the existence of two compounds, $CaHf_4O_9$ and $CaHfO_3$. A more comprehensive study on the ordered phenomena in this system was then done by Allpress and co-workers [154–156]. These authors described three ordered phases:

- (i) $CaHf_4O_9$ (ϕ_1), which had a monoclinic (C/2c) structure and formed at 20 mol % CaO;
- (ii) $Ca_2Hf_7O_{16}$ (ϕ), which had a rhombohedral (R3c) structure and formed at 22.22 mol % CaO; and
- (iii) $Ca_6Hf_{19}O_{44}$ (ϕ_2), which also had a rhombohedral (R3c) structure but formed at 24 mol % CaO.

Recently, Stubican and co-workers [85, 149] further studied the phase relationships in the HfO_2 -CaO system in order to establish the stability limits for each of the solid solutions and all possible compounds. On the basis of their experimental results and those obtained by the previous investigators, they proposed the diagram shown in Fig. 11 for the HfO_2 -rich portion of this system. The solubility of CaO in monoclinic and tetragonal HfO_2 is very low, less than 0.5 mol %. The transformation temperatures for both the cubic to tetragonal and the tetragonal to monoclinic are lowered by the CaO alloying in HfO_2 . Cubic

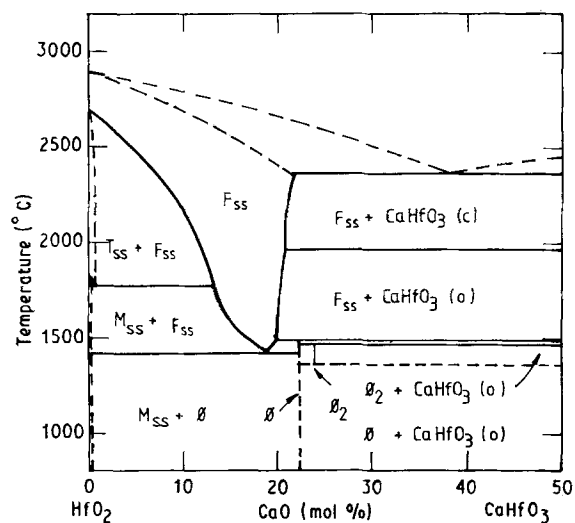


Figure 11 The phase relationships in the HfO_2 -CaO system proposed by Senft and Stubican [85, 149] for the HfO_2 -rich portion. $CaHf_4O_9$ (ϕ_1) is not shown in this diagram.

HfO₂ solid solution (F_{ss}, fluorite-type structure) is stable at temperatures above 1415 ± 7 °C. The eutectoid decomposition point between the tetragonal solid solution region (T_{ss}) and the monoclinic (M_{ss}) + cubic (F_{ss}) two-phase region is at < 0.5 mol % CaO and 1775 ± 50 °C. The transition temperature for the CaHfO₃ (orthorhombic)–CaHfO₃ (cubic) is 1955 ± 40 °C. The eutectoid decomposition point for the cubic solid solution is at 19.0 ± 0.5 mol % CaO and at 1415 ± 7 °C.

Although Stubican and co-workers [85, 149] did not work out the exact stability limits for each possible ordered compound in this system, they believed the results obtained by the previous researchers, such as Allpress and co-workers [154–156]. The ordered compound CaHF₄O₉ (corresponding to CaZr₄O₉ in the ZrO₂–CaO system [149]), which is not indicated in the diagram, is metastable at all temperatures. It decomposes into an HfO₂ solid solution and the Ca₂Hf₇O₁₆ (ϕ) phase, which is stable with an upper limit of 1470 ± 50 °C. The compound Ca₆Hf₁₉O₄₄, which is shown as ϕ₂ in Fig. 11, is stable from 1350 ± 50 °C to its upper limit of 1460 °C.

6.3.3. The HfO₂–MgO system

The phase relationships in the HfO₂–MgO system have been established, to a large extent, by a few research scientists in the Commonwealth of Independent States [110, 148, 157–159]. Fig. 12 is one of the diagrams constructed by Lopato *et al.* [159]. The addition of MgO to HfO₂ stabilizes the cubic and tetragonal phases as it does to ZrO₂ [160], resulting in a decrease in the temperature for the tetragonal to monoclinic transformation. As an example, 3 mol % MgO alloying will result in a 100 °C decrease in the transformation temperature (from 1800 °C for undoped HfO₂ to 1700 °C for 3 mol % MgO-doped HfO₂). The unit cells of tetragonal and cubic HfO₂ solid solutions (T_{ss} and F_{ss}) decrease with increasing MgO alloying, a consequence of relative smaller size of Mg²⁺ (0.066 nm) in comparison with that of Hf⁴⁺ (0.083 nm) [32]. The diagram contains three eutectoid points:

- (i) at 50 mol % MgO and at 2100 °C;
- (ii) at 18 mol % MgO and at 1500 °C; and
- (iii) at 4.5 mol % MgO and at 1725 °C.

It is very interesting to compare that the second eutectoid decomposition above corresponds to the eutectoid point at 13 mol % MgO and at 1400 °C in the ZrO₂–MgO system [160]. The monoclinic and tetragonal HfO₂ solid solutions are limited to the compositions containing less than 3 and 4 mol % MgO, respectively. The solubility of HfO₂ in MgO is 1 mol %. Although the diagram does not contain any ordered phases, the existence of Mg₂Hf₅O₁₂ with a rhombohedral structure (*a* = 0.6148 nm, β = 99°35′) was detected by Gavriš and Zoz [161] and by Delamarre [157]. This compound corresponds to Mg₂Zr₅O₁₂ in the ZrO₂–MgO system [160].

Of the most interest in the HfO₂–MgO system is the solid solution of cubic HfO₂ modification, which decomposes to a monoclinic solid solution (M_{ss}) and free

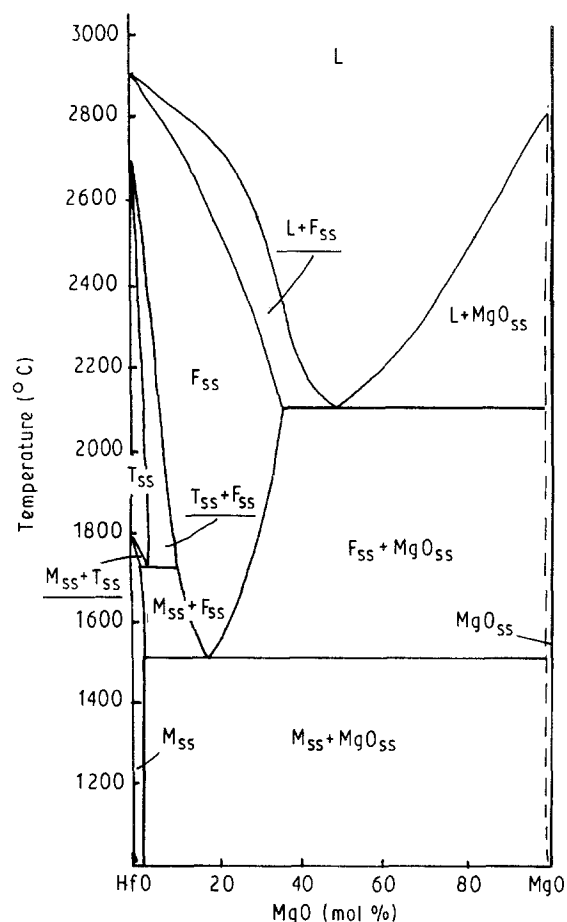


Figure 12 The phase diagram proposed for the HfO₂–MgO system by Lopato *et al.* [159]. The solubility of MgO in monoclinic HfO₂ and tetragonal HfO₂ solid solutions is 3 and 4 mol %, respectively.

MgO at temperatures below 1500 °C. The resultant free MgO precipitation particles are concentrated at the grain boundaries of the original cubic solid solution [111]. The corresponding decomposition reaction in the ZrO₂–MgO system occurs at 12.8 mol % MgO and at 1400 °C to form free MgO and a tetragonal solid solution which transforms to a monoclinic ZrO₂ solid solution at 1240 °C [160].

6.3.4. The HfO₂–Y₂O₃ system

The most recently constructed phase diagram for the HfO₂–Y₂O₃ system is due to Stubican [162], Fig. 13. The following features can be summarized from the diagram, when compared with that for the ZrO₂–Y₂O₃ system [162, 163].

(i) The monoclinic solid solution (M_{ss}) is restricted to < 2 mol % Y₂O₃ and the tetragonal solid solution (T_{ss}) to < 3 mol % Y₂O₃ at 1600 °C. These solubility limits are very similar to those in the ZrO₂–Y₂O₃ system, in which the tetragonal solid solution exists up to 2.5 mol % Y₂O₃.

(ii) The cubic solid solution (F_{ss}) occupies a wide composition range, e.g. 15–50 mol % Y₂O₃ at 1500 °C and 10–55 mol % Y₂O₃ at 1800 °C.

(iii) The temperatures for both the cubic to tetragonal and the tetragonal to monoclinic transformations are lowered by the Y₂O₃ alloying in HfO₂.

(iv) The eutectoid decomposition temperature (1350 °C) is considerably higher than that in the ZrO₂–Y₂O₃ system (550 °C) [163].

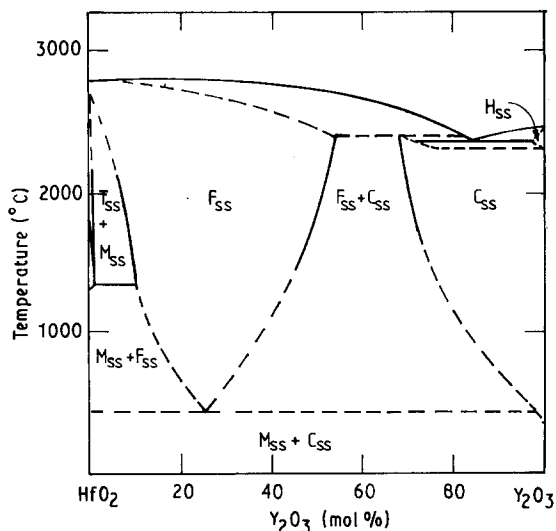


Figure 13 The phase relationships in the $\text{HfO}_2\text{-Y}_2\text{O}_3$ system suggested by Stubican [162]. A limited amount of Y_2O_3 is soluble in monoclinic and tetragonal HfO_2 solid solutions. No ordered compounds are observed in this system. C_{ss} and H_{ss} are the cubic and hexagonal Y_2O_3 solid solutions, respectively.

(v) It is unlikely that the $\text{HfO}_2\text{-Y}_2\text{O}_3$ system contains any ordered compounds, as no such evidence was found in the compositions containing 10–75 mol % Y_2O_3 , which were held at 1300 and 1400 °C for up to 6 months.

In contrast, a well-documented compound, $\text{Y}_4\text{Zr}_3\text{O}_{12}$, exists in the $\text{ZrO}_2\text{-Y}_2\text{O}_3$ system. The existence of compounds $\text{Y}_2\text{Hf}_2\text{O}_7$ and $\text{Y}_2\text{Hf}_7\text{O}_{17}$ with the fluorite-type structure was indeed observed by Caillet *et al.* [164] and by Duclot *et al.* [165] in the $\text{HfO}_2\text{-Y}_2\text{O}_3$ system. Furthermore, the formation of a metastable compound $\text{Y}_2\text{Hf}_3\text{O}_{12}$, which had an associated solid solution range of 33–50 mol % Y_2O_3 and transformed to a fluorite-type phase at 1350 °C, was also detected by these authors. However, these results could not be reproduced by other investigators.

6.3.5. The $\text{HfO}_2\text{-Yb}_2\text{O}_3$ system

Certain compositions in the $\text{HfO}_2\text{-Yb}_2\text{O}_3$ system exhibit useful thermal properties for engineering applications. The thermal expansion coefficient of Yb_2O_3 -doped HfO_2 ceramics is higher than that of monolithic HfO_2 ceramics. In the composition range 2–10 mol % Yb_2O_3 , their thermal expansion coefficient increases with increasing Yb_2O_3 content.

Following the early work by Perez y Jorba [166], Rouanet [167], and Corman and Stubican [168], Duran and Pascual [109] studied the phase relationships in the $\text{HfO}_2\text{-Yb}_2\text{O}_3$ system and proposed a diagram as shown in Fig. 14. The monoclinic solid solution (M_{ss}) region exists from 0–1 mol % Yb_2O_3 at room temperature and from 0–1.5 mol % at 1590 °C. There exists only a limited tetragonal solid solution (T_{ss}) region (up to 3 mol % Yb_2O_3) at temperatures above 1600 °C. The Yb_2O_3 alloying in HfO_2 results in a decrease in the tetragonal to monoclinic transformation temperature and an increase in the lattice parameters of HfO_2 . The boundaries between the cubic and the cubic + tetragonal two-phase regions

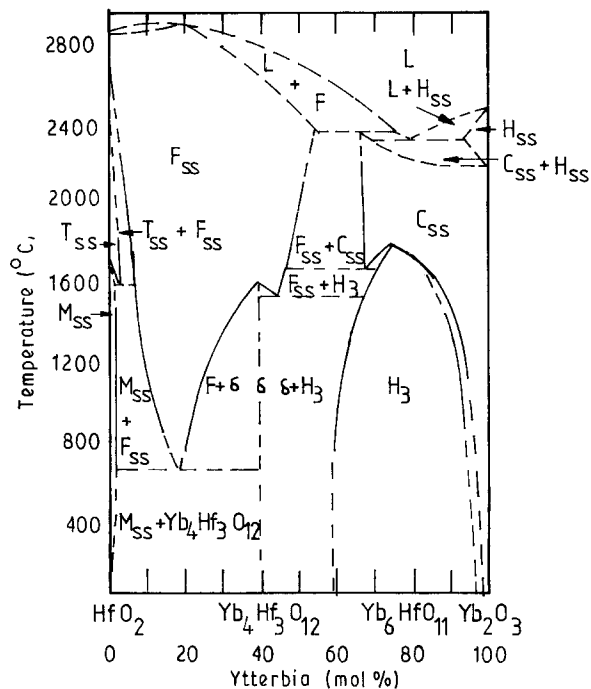


Figure 14 The phase diagram for the $\text{HfO}_2\text{-Yb}_2\text{O}_3$ system proposed by Duran and Pascual [109]. M_{ss} , T_{ss} and F_{ss} are monoclinic, tetragonal and cubic hafnia solid solutions, respectively. C_{ss} is cubic Yb_2O_3 solid solution. δ is the hexagonal compound $\text{Yb}_4\text{Hf}_3\text{O}_{12}$; H_3 is the hexagonal compound $\text{Yb}_6\text{HfO}_{11}$. C_{ss} and H_{ss} are the cubic and hexagonal Yb_2O_3 solid solutions, respectively.

are: 14 mol % Yb_2O_3 at 800 °C, 12 mol % Yb_2O_3 at 1000 °C, 10 mol % Yb_2O_3 at 1200 °C, 9 mol % Yb_2O_3 at 1400 °C, 7 mol % Yb_2O_3 at 1600 °C, 6 mol % Yb_2O_3 at 1700 °C, 5 mol % Yb_2O_3 at 2000 °C, and 3.5 mol % Yb_2O_3 at 2200 °C. The cubic solid solution (F_{ss}) region exists from 14–20 mol % Yb_2O_3 at 800 °C and from 3.5–54 mol % Yb_2O_3 at 2200 °C.

From 55–67 mol % Yb_2O_3 , there exists a further two-phase region near the solidus: HfO_2 solid solution (fluorite-type phase) and cubic Yb_2O_3 solid solution (C-type phase). This two-phase region widens to 69 mol % Yb_2O_3 at 1700 °C. The single Yb_2O_3 solid solution phase region exists from pure Yb_2O_3 to 33 mol % HfO_2 at 2200 °C, and to 31 mol % HfO_2 at 1800 °C.

Two hexagonal phases, $\text{Yb}_4\text{Hf}_3\text{O}_{12}$ (δ) and $\text{Yb}_6\text{HfO}_{11}$ (H_3), exist at temperatures below 1800 °C in this system; they were observed to occur at 40 and 70 mol % Yb_2O_3 , respectively. The former, which exhibits a similar structure to $\text{Yb}_4\text{Zr}_3\text{O}_{12}$, has a unit cell of $a = 0.9614$ nm and $c = 1.7908$ nm. Its formation occurs more readily than the formation of corresponding compounds in any other $\text{HfO}_2\text{-Ln}_2\text{O}_3$ systems [148, 169, 170]. The compound $\text{Yb}_6\text{HfO}_{11}$, which is stable up to 1750 ± 50 °C and has a solid solution region of 58–95 mol % Yb_2O_3 , also has a hexagonal unit cell of $a = 0.9647$ nm and $c = 1.8204$ nm. Both $\text{Yb}_4\text{Hf}_3\text{O}_{12}$ and $\text{Yb}_6\text{HfO}_{11}$ could be decomposed into a cubic solid solution and a C-type solid solution by an order–disorder process. Duran and Pascual [109], however, did not observe the existence of a third hexagonal phase of the $\text{YbHf}_5\text{O}_{11.5}$ type, although it was noted by Perez y Jorba [166]. Further investigation is probably needed in order to prove its existence,

as a modified phase of either $\text{Yb}_4\text{Hf}_3\text{O}_{12}$ or $\text{Yb}_6\text{HfO}_{11}$. As is illustrated in Fig. 14, there exist five invariant points in the $\text{HfO}_2\text{-Yb}_2\text{O}_3$ system at 660, 1530, 1590, 1680 and 2380 °C, respectively. Amongst these invariant points, the first four are eutectoid type and the last one is a peritectic type.

6.3.6. The $\text{HfO}_2\text{-Er}_2\text{O}_3$ system

A limited amount of work has been done on the phase relationships in the $\text{HfO}_2\text{-Er}_2\text{O}_3$ system [171–173]. The first major contribution to the understanding of this system was due to Spiridonov and Komissarova [171].

Very recently, Duran *et al.* [174] studied this system using thermal expansion measurement and X-ray diffraction, and obtained the results shown in Fig. 15. The solubility of Er_2O_3 in HfO_2 is < 2.5 mol % at temperatures below 1650 °C. The tetragonal solid solution (T_{ss}) region occupies the composition range 0–6 mol % Er_2O_3 at 2000 °C. The cubic solid solution (F_{ss}) single-phase region occupies a wide composition range, e.g. 8–50 mol % Er_2O_3 at 2000 °C. These results agreed well with those of Spiridonov and Komissarova [171]. Three compounds all with hexagonal structure exist in this system:

(i) $\text{Er}_4\text{Hf}_3\text{O}_{12}$ (δ , $a = 0.9709$ nm, $c = 1.8042$ nm), which forms at 40 mol % Er_2O_3 and decomposes at 1500 °C into a cubic solid solution;

(ii) $\text{Er}_3\text{Hf}_2\text{O}_{11.5}$ (H_2 , $a = 0.9737$ nm, $c = 1.8106$ nm), which forms at 55 mol % Er_2O_3 and undergoes a phase transformation at 1650 °C and then decomposes into HfO_2 and Er_2O_3 -based cubic solid solutions; and

(iii) $\text{Er}_6\text{HfO}_{11}$ (H_3 , $a = 0.9790$ nm, $c = 1.8456$ nm), which was first reported by Spiridonov and Komissarova [171] and decomposes into HfO_2 and Er_2O_3 -based solid solutions at temperatures above 1700 °C.

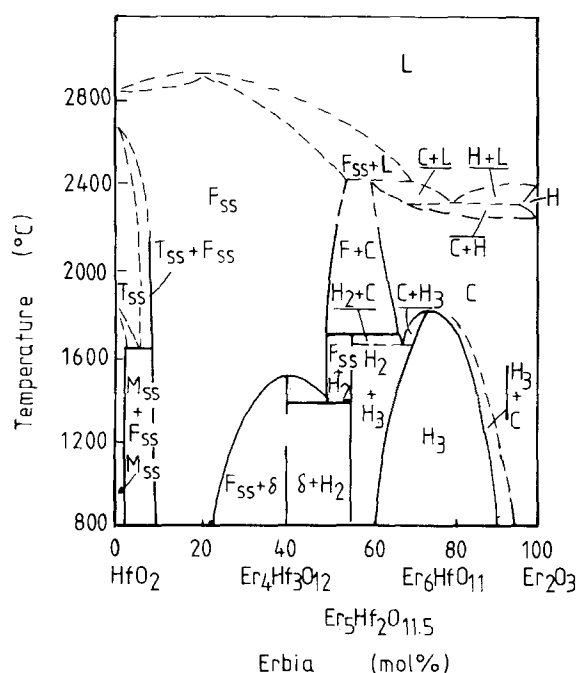


Figure 15 The phase diagram proposed for the $\text{HfO}_2\text{-Er}_2\text{O}_3$ system by Duran *et al.* [174]. δ , H_2 and H_3 refer to $\text{Er}_4\text{Hf}_3\text{O}_{12}$, $\text{Er}_3\text{Hf}_2\text{O}_{11.5}$, $\text{Er}_6\text{HfO}_{11}$, respectively. C_{ss} and H_{ss} are the cubic and hexagonal Er_2O_3 solid solutions, respectively.

6.3.7. The $\text{HfO}_2\text{-CeO}_2$ system

The $\text{HfO}_2\text{-CeO}_2$ system has been studied much less in comparison to its counterpart in the ZrO_2 based systems, i.e. the $\text{ZrO}_2\text{-CeO}_2$ system [175]. The preliminary results are due to a few research scientists in the Commonwealth of Independent States [176, 177]. Fig. 16 is one of the phase diagrams worked out for this system by these scientists, whose results were mainly obtained using X-ray powder diffraction. The samples they investigated were mixed $\text{HfO}_2\text{-CeO}_2$ powders, prepared by calcining coprecipitated Zr–Ce hydroxides at temperatures of 1000–1500 °C for various periods of time. The formation of monoclinic, and cubic solid solutions (M_{ss} and F_{ss}) was observed to occur in this system. However, no evidence was observed for the existence of either tetragonal solid solution (T_{ss}) or any ordered compounds. It is apparent that a substantial amount of further research work is needed in order to understand fully the phase relationships in the $\text{HfO}_2\text{-CeO}_2$ system, which could be technologically important if toughened ceramics similar to those in the $\text{ZrO}_2\text{-CeO}_2$ system can be obtained [178].

6.3.8. The $\text{HfO}_2\text{-TiO}_2$ system

There has been considerable interest in certain $\text{HfO}_2\text{-TiO}_2$ compositions because of their low thermal expansion coefficients. Simpson [179] reported that compositions containing 30–50 mol % TiO_2 had zero or a slightly negative coefficient of thermal expansion. This was followed by an extensive investigation into the $\text{HfO}_2\text{-TiO}_2$ system by a number of researchers [180–186].

The most comprehensive investigations into this system made so far are due to Ruh *et al.* [186] and Coutures and Coutures [187], who used X-ray diffraction and thermal analysis as experimental techniques. Fig. 17 is a tentative phase diagram suggested by these authors for the $\text{HfO}_2\text{-TiO}_2$ system. It is seen that the solubility of TiO_2 in monoclinic HfO_2 solid solution (M_{ss}) is relatively high, 10.0 mol % at 1570 ± 20 °C. Within the solubility limit, the unit cell of monoclinic HfO_2 solid solution decreases with increasing TiO_2 addition, as was indicated by the interplanar spacing measurement [187, 188]. The solubility of TiO_2 in

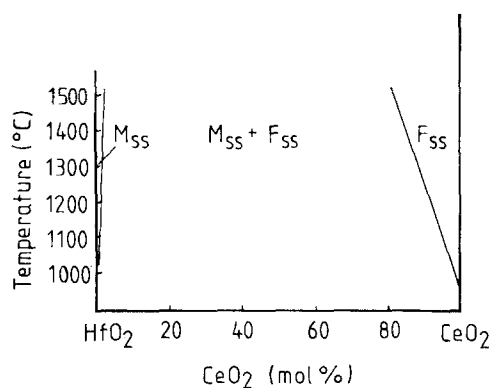


Figure 16 The phase relationships in the $\text{HfO}_2\text{-CeO}_2$ system worked out by Spiridonov *et al.* [177]. No tetragonal solid solution and ordered compounds were observed to occur in this system.

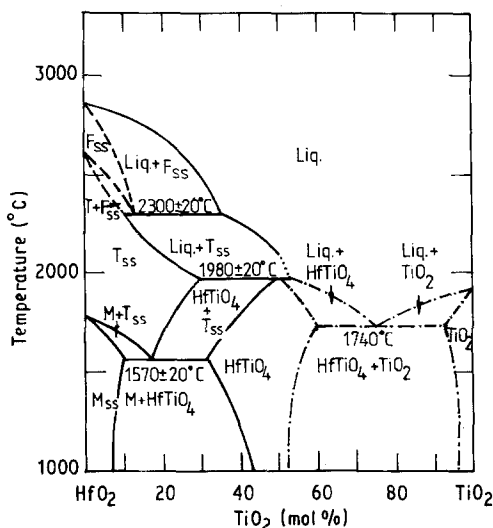


Figure 17 A tentative phase diagram for the HfO_2 - TiO_2 system by Coutures *et al.* [187]. There exists an extended tetragonal single-phase region and an ordered compound, HfTiO_4 , in this system. The HfTiO_4 -based compositions exhibit a very low thermal expansion coefficient.

tetragonal HfO_2 solid solution (T_{ss}) extends up to 24 mol% at 1700 °C and to 30 mol% at 2000 °C. Therefore, this tetragonal HfO_2 solid solution region is the widest one existing in the HfO_2 based systems. The electrical conductivity and fracture strength of these HfO_2 solid solutions increases with increasing TiO_2 content.

With further increase in TiO_2 content beyond the solubility limit, there follows the formation of an orthorhombic hafnium titanate, HfTiO_4 . The monoclinic solid solution and hafnium titanate two-phase region occupies the composition range from 10–36 mol% TiO_2 at 1400 °C. The unit cell of the monoclinic HfO_2 solid solution is almost unchanged with increasing TiO_2 as soon as HfTiO_4 forms. The single-phase HfTiO_4 solid solution, whose definite compound HfTiO_4 melts incongruently at $1980 \pm 10^\circ\text{C}$ and at 53 mol% TiO_2 , has the composition range of 43–52 mol% TiO_2 at 1000 °C and 35–56 mol% TiO_2 at 1600 °C. A metatectic forms at 35 mol% TiO_2 and at $2300 \pm 20^\circ\text{C}$. The eutectoid decomposition of $\text{HfO}_2(t)_{ss} \rightarrow \text{HfO}_2(m)_{ss} + \text{HfTiO}_4(\text{orth})_{ss}$ occurs at 18.5 mol% TiO_2 and at $1570 \pm 20^\circ\text{C}$. On the right-hand side of the phase diagram, a wide field of HfTiO_4 and TiO_2 solid solution two-phase region exists and the solubility of HfO_2 in TiO_2 is 8 mol% at 1700 °C. The eutectic decomposition on this side occurs at 25 mol% HfO_2 and at $1740 \pm 10^\circ\text{C}$.

As discussed above, HfTiO_4 -based compositions are technologically important in terms of their low thermal expansion coefficients. It is therefore worth presenting a brief account to their microstructure, and mechanical and thermal properties. Historically, Godina *et al.* [180] first observed the existence of an orthorhombic compound HfTiO_4 in the HfO_2 - TiO_2 system. Its crystal structure, polymorphism, thermal and mechanical properties were further investigated by Harari *et al.* [181], Lynch and Morosin [182], Mazdiyasi and Brown [183], and Ruh *et al.* [186]. It has a space group of pbcn with Hf^{4+} and Ti^{4+} ions in

random order on the metal sites. Its lattice parameters are dependent on composition and temperature. Fig. 18 is an example which shows the temperature dependence of the lattice parameters for HfTiO_4 solid solutions containing 45 and 50 mol% TiO_2 , respectively.

The thermal expansion of HfTiO_4 is highly anisotropic. The expansions in the a - and b -axes are substantial and that in the c -axis is very low. The overall low thermal expansion of polycrystalline HfTiO_4 ceramics is therefore due to the extensive microcracks occurring in sintered bodies. The driving force for the microcracking is the residual strain energy associated with the anisotropic thermal expansion stresses. It is thus concluded that grain size has a strong effect on the thermal and mechanical properties of HfTiO_4 based materials as it is one of the determining parameters for the level of residual strain energy formed in anisotropic materials [208].

The mechanical properties, such as flexure strength, microhardness, Young's modulus and fracture energy, of several HfTiO_4 based compositions were studied by Hollenberg *et al.* [184], and Canadien [188]. The grain size of the materials they investigated were in the range 2–10 μm . The fracture strength was observed to be nearly unchanged in the composition region of 30–40 mol% TiO_2 (40–80 MPa) and to increase by a factor of 2 in the composition region 45–50 mol% TiO_2 with increasing TiO_2 content. The fracture strength increased with increasing temperature from room temperature to 1100 °C, and then decreased as the temperature increased further. The fracture energy decreased slightly with increasing TiO_2 content in the composition region 30–50 mol% TiO_2 . The microhardness was in the range 3.3–7.2 GPa, increasing slightly with increasing TiO_2 content, although the porosity level in these sintered specimens increased as well [184, 188].

6.3.9. The HfO_2 - ZrO_2 system

Because they are strikingly similar in crystal structure

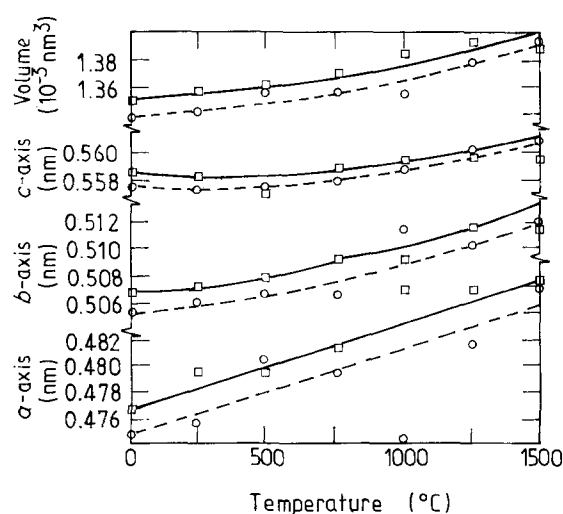


Figure 18 The lattice parameters as a function of temperature for two HfTiO_4 -based compositions containing (—□—) 45 and (---○---) 50 mol% TiO_2 , respectively. The thermal expansions in the a - and b -axes are substantial and that in the c -axis is very low [187].

TABLE VII The tetragonal \rightleftharpoons monoclinic transformation temperatures for HfO₂-ZrO₂ solid solutions determined by DTA [30]

Composition	Mono. to tetr. (°C)		Tetr. to mono. (°C)	
	Starting	Completion	Starting	Completion
ZrO ₂	1160	1215	1038	993
ZrO ₂ -10 wt % HfO ₂	1204	1273	1104	1028
ZrO ₂ -20 wt % HfO ₂	1244	1303	1154	1087
ZrO ₂ -30 wt % HfO ₂	1294	1368	1220	1126
ZrO ₂ -40 wt % HfO ₂	1380	1453	1318	1275
ZrO ₂ -50 wt % HfO ₂	1421	1470	1348	1282
ZrO ₂ -60 wt % HfO ₂	1496	1570	1428	1380
ZrO ₂ -70 wt % HfO ₂	1526	1595	1455	1397
ZrO ₂ -80 wt % HfO ₂	1589	1657	1542	1490
ZrO ₂ -90 wt % HfO ₂	1674	1707	1626	1582
HfO ₂	1750	1775	1695	1645

and phase transformation, HfO₂ and ZrO₂ form a continuous solid solution over the entire range of composition. Historically, hafnium had not been recognized until 1923 [26], almost 134 years after zirconium was first discovered in 1789. The systematic studies on the structure, phase transformation and properties of HfO₂-ZrO₂ solid solutions had not been carried out until the 1950s.

Curtis *et al.* [80] first examined the solid solutions in the HfO₂-ZrO₂ system using X-ray diffraction, and found a gradual decrease in the interplanar spacing with increasing HfO₂ alloying. This was correctly interpreted as being due to a continuous solid solution which was formed in the system and that the unit cell of monoclinic HfO₂ was slightly smaller than that of monoclinic ZrO₂. Stansfield [189] investigated the monoclinic to tetragonal transformation in mixed HfO₂-ZrO₂ compositions using thermal expansion measurement and noted that the transformation temperature decreased almost linearly in moving from HfO₂ to ZrO₂.

A detailed study on the phase relationships in the HfO₂-ZrO₂ system was first made by Ruh *et al.* [30] and more recently by Shevchenko *et al.* [112], using techniques such as metallographic analysis, X-ray diffraction (XRD), differential thermal analysis (DTA), melting-point measurement, and microprobe analysis. Specifically, Ruh *et al.* [30] obtained the detailed information at relatively low temperatures and Shevchenko *et al.* [112] obtained further information at relatively high temperatures (up to 2800 °C). The diagram constructed by Shevchenko *et al.* [112] is shown in Fig. 19.

It is a characteristic of the HfO₂-ZrO₂ system to form continuous solid solutions based on monoclinic, tetragonal and cubic modifications (M_{ss}, T_{ss}, and F_{ss}) of the original components. The following summary can be made on the basis of this phase diagram, when composition moves towards HfO₂:

(i) an almost linear rise in the transformation temperature both for the monoclinic to tetragonal, Table VII, and the tetragonal to cubic;

(ii) a continuous rise (almost linearly) in the melting point of solid solution, Table VIII;

(iii) there probably exist three lens-shaped two-phase regions: monoclinic HfO₂ solid solution + tetragonal ZrO₂ solid solution; tetragonal HfO₂ solid

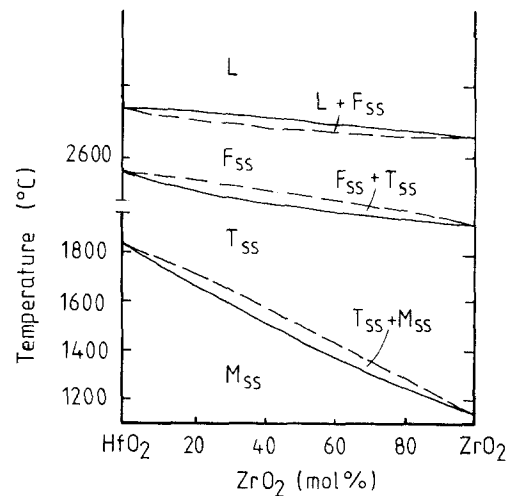


Figure 19 The phase relationships in the HfO₂-ZrO₂ system suggested by Shevchenko *et al.* [112], illustrating a complete solubility of HfO₂ in ZrO₂. The transformation temperatures of HfO₂-ZrO₂ solid solution obey approximately the rule of mixtures.

TABLE VIII The melting points of HfO₂-ZrO₂ solid solutions [30]

Composition	Melting point (°C)
ZrO ₂	2690
ZrO ₂ -10 wt % HfO ₂	2730
ZrO ₂ -20 wt % HfO ₂	2735
ZrO ₂ -30 wt % HfO ₂	2745
ZrO ₂ -40 wt % HfO ₂	2750
ZrO ₂ -50 wt % HfO ₂	2780
ZrO ₂ -60 wt % HfO ₂	2790
ZrO ₂ -70 wt % HfO ₂	2810
ZrO ₂ -80 wt % HfO ₂	2825
ZrO ₂ -90 wt % HfO ₂	2860
HfO ₂	2900

solution + cubic ZrO₂ solid solution; and cubic HfO₂ solid solution + liquid ZrO₂, respectively.

In comparison with Fig. 19, the phase diagram suggested by Ruh *et al.* [30] did not show the existence of a lens-shaped monoclinic HfO₂ solid solution + tetragonal ZrO₂ solid solution two-phase region, although they recognized a slight decrease in the size of the temperature hysteresis for the monoclinic \rightleftharpoons tetragonal transformations. In an independent investigation into the anomalous thermal expansion in the Al₂O₃/15 vol % Hf_{0.5}Zr_{0.5}O₂ composite, Kriven and

TABLE IX The lattice parameters of monoclinic HfO₂-ZrO₂ solid solutions [30]

Composition and heat treatment temperature	Parameters (nm)			β (deg)	Volume, V (nm ³)
	a	b	c		
ZrO ₂ (room temp.)	0.5159	0.5204	0.5324	99.03	0.14116
ZrO ₂ (1000°C)	0.5140	0.5200	0.5310	99.24	0.14008
ZrO ₂ -20 wt % HfO ₂ (1000°C)	0.5133	0.5179	0.5301	99.27	0.13980
ZrO ₂ -40 wt % HfO ₂ (1000°C)	0.5127	0.5177	0.5299	99.28	0.13880
ZrO ₂ -60 wt % HfO ₂ (1000°C)	0.5126	0.5171	0.5297	99.28	0.13857
ZrO ₂ -80 wt % HfO ₂ (1000°C)	0.5123	0.5170	0.5294	99.14	0.13843
HfO ₂ (1000°C)	0.5128	0.5167	0.5294	99.18	0.13848
HfO ₂ (room temp.)	0.5119	0.5169	0.5290	99.25	0.13821

TABLE X The average linear thermal expansion coefficients of HfO₂-ZrO₂ solid solutions

Composition Hf _{1-x} Zr _x O ₂	Average thermal expansion coefficient (10 ⁻⁶ °C ⁻¹)	Temperature range (°C)	Reference
0.00	6.5	25-1200	[191]
0.22	7.2	900-1550	[189]
	12.1	1600-2250	-
0.31	7.3	900-1550	-
	12.2	1700-2200	-
0.51	7.2	900-1300	-
	13.9	1450-2450	-
0.71	7.4	900-1250	-
	15.1	1450-2400	-
1.00	8.0	25-1500	[80]

Bischoff [190] confirmed the existence of the lens-shaped monoclinic HfO₂ solid solution + tetragonal ZrO₂ solid solution two-phase region.

As will be discussed below, HfO₂-ZrO₂ solid solutions are considered useful in toughening engineering ceramics for structural applications in the intermediate temperature range. Their unit cell dimensions, as shown in Table IX and Fig. 20, characteristics associated with the tetragonal to monoclinic phase transformation, thermal, and physical properties obey approximately the rule of mixtures. For example, there is a slight decrease in the thermal expansion coefficient of the solid solution with increasing HfO₂ alloying, as shown in Table X. The critical grain size for retaining metastable tetragonal phase in the solid solution also decreases when the composition moves towards HfO₂.

6.3.10. The HfO₂-ZrO₂-Y₂O₃ system

Although investigations have been carried out for the phase relationships in the relevant binary phase systems, those in the ternary HfO₂-ZrO₂-Y₂O₃ system have not been paid very much attention. Only very recently, a preliminary study was made by Trubelja and Stubican [192], who constructed two ternary phase diagrams for this system at 1300 and 1600 °C, respectively. Fig. 21 is the one at 1600 °C. There exists a large cubic solid solution (F_{ss}) region at this temperature. Along the 15 mol % ZrO₂ join, the cubic solid solution phase exists from 11.5-45.5 mol % Y₂O₃, compared with the composition range from 12-43

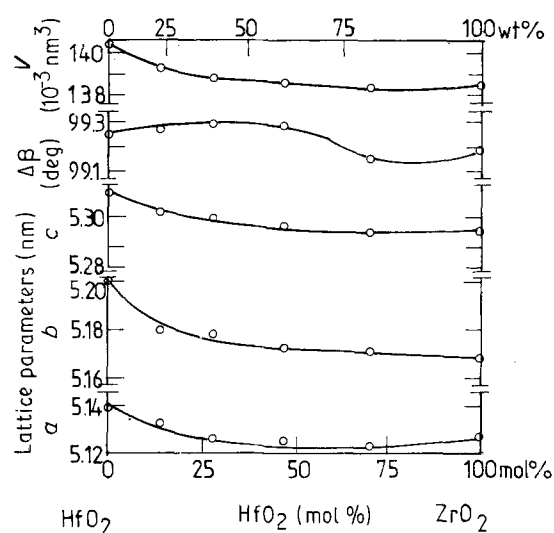


Figure 20 The lattice parameters of HfO₂-ZrO₂ solid solution as a function of composition. The samples were annealed and quenched from 1000 °C [30].

mol % Y₂O₃ at 1300 °C. Along the 15 mol % HfO₂ join, the cubic solid solution phase region occupies the composition range from 7.5-45 mol % Y₂O₃, compared with that from 8-39 mol % Y₂O₃ at 1300 °C. An ordered phase, which is similar to that (Zr₃Y₄O₁₂) formed at 40 mol % Y₂O₃ in the ZrO₂-Y₂O₃ system [163], was observed at 1300 °C in the compositions containing less than 15 mol % HfO₂. Further addition of HfO₂ seemed to inhibit the formation of this ordered phase. This observation is consistent with the

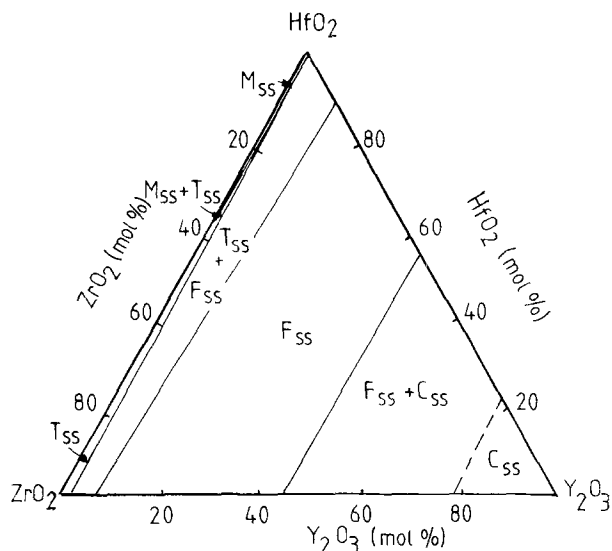


Figure 21 The phase relationships in the $\text{HfO}_2\text{-ZrO}_2\text{-Y}_2\text{O}_3$ system at 1600°C , proposed by Trubelja and Stubican [192]. C_{ss} is Y_2O_3 -based solid solution.

results obtained in the relevant binary $\text{ZrO}_2\text{-Y}_2\text{O}_3$ and $\text{HfO}_2\text{-Y}_2\text{O}_3$ systems. As was discussed above, it is unlikely that there exist any ordered compounds in the $\text{HfO}_2\text{-Y}_2\text{O}_3$ system [162], whereas an ordered compound, $\text{Zr}_3\text{Y}_4\text{O}_7$, has been found to occur in the $\text{ZrO}_2\text{-Y}_2\text{O}_3$ system [163].

Certain compositions in the ternary $\text{HfO}_2\text{-ZrO}_2\text{-Y}_2\text{O}_3$ system may be considerably useful in developing transformation-toughened ceramics. The presence of either ZrO_2 or Y_2O_3 will result in a modification in the characteristics of the tetragonal to monoclinic transformation in HfO_2 , such as the transformation starting temperature, the critical grain size for retaining the metastable tetragonal phase, the volume expansion and the shear strain associated with the transformation. Further investigation is needed in order to understand fully the relationships between composition and these parameters in this ternary system.

7. HfO_2 and $\text{HfO}_2\text{-ZrO}_2$ solid solutions as toughening agents

Strictly speaking, $\text{HfO}_2\text{-ZrO}_2$ solid solutions are the most widely utilized toughening agent in structural ceramics [40, 41], as commercial ZrO_2 sources almost always contain 2–3 wt % HfO_2 as an integral impurity. In other words, most of ZrO_2 -toughened ceramics are, in fact, $\text{HfO}_2\text{-ZrO}_2$ solid solution toughened ceramics. When one considers HfO_2 and the high HfO_2 -containing ZrO_2 solid solutions as potential toughening agents, it is important to know their likely advantages and disadvantages, in comparison with ZrO_2 .

The most significant advantage in using HfO_2 as a toughening agent in structural ceramics is the possibility of obtaining transformation toughening at elevated temperatures. For ZrO_2 toughened ceramics, the potential applications are limited by the low tetragonal (ZrO_2) to monoclinic (ZrO_2) transformation temperature, which is approximately 1000°C . In contrast, HfO_2 exhibits a much higher transformation temperature ($\sim 1700^\circ\text{C}$) than ZrO_2 . It is therefore theoret-

ically possible to utilize toughening mechanisms such as stress-induced transformation and compressive surface stress generation at temperatures up to 1700°C in HfO_2 -toughened ceramics. Consequently it is easy to understand why HfO_2 has been widely suggested as being a useful substitute material for ZrO_2 at high temperatures. Similarly, HfO_2 is also considered by some ceramists to be a more effective toughening agent at room temperature than is ZrO_2 , due to the increased free energy change associated with the tetragonal to monoclinic transformation [107, 108].

The temperature for the tetragonal to monoclinic transformation in $\text{HfO}_2\text{-ZrO}_2$ solid solutions is dependent on their composition, increasing almost linearly with increasing HfO_2 content [30, 112], as shown in Fig. 19 and Table VII. As an example, the tetragonal to monoclinic transformation starts at 1348°C and completes at 1282°C in $\text{ZrO}_2\text{-50 wt % HfO}_2$, compared with 1038 and 993°C , respectively, for monolithic ZrO_2 . In an independent study, Claussen *et al.* [193] and Kriven and Bischoff [190] observed that the starting temperature of the monoclinic to tetragonal transition was to shift to 1460°C for the $\text{Hf}_{0.5}\text{Zr}_{0.5}\text{O}_2$ solid solution constrained in an Al_2O_3 matrix, indicating the increased tetragonal to monoclinic transformation temperatures in $\text{HfO}_2\text{-ZrO}_2$ solid solutions over pure ZrO_2 . The composition of a $\text{HfO}_2\text{-ZrO}_2$ solid solution will therefore determine the maximum temperature up to which transformation toughening and compressive surface stresses can be retained.

However, there are certain disadvantages in using HfO_2 and $\text{HfO}_2\text{-ZrO}_2$ solid solutions as toughening agents for structural ceramics. According to Evans and co-worker [130–132], the amounts of the volume expansion and shear strain associated with the tetragonal to monoclinic transformation are vital in determining the toughness increment. Unfortunately, the volume expansion and shear strains associated with the tetragonal to monoclinic transformation in HfO_2 are lower than those in ZrO_2 [80, 96, 121]. $\text{HfO}_2\text{-ZrO}_2$ solid solutions have a similar disadvantage, the degree depending on their composition.

The second disadvantage in using HfO_2 for transformation toughening is concerned with the difficulties experienced in retaining the metastable tetragonal phase in ceramic matrices in terms of its small critical grain size. As was mentioned earlier, the critical grain size for strain-free HfO_2 (4–10 nm) is much smaller than that for ZrO_2 (15–30 nm) [122–124]. Although the constraint applied by a sintered matrix may result in an increase in the critical grain size, it is almost impossible to obtain fine grain sized HfO_2 inclusions of less than 50 nm in a sintered ceramic matrix via the conventional sintering of mixed ceramic powder compacts. Using $\text{HfO}_2\text{-ZrO}_2$ solid solutions as toughening agents, one will face similar difficulties, although the critical grain size increases with increasing ZrO_2 content. As an example, Claussen *et al.* [193] and Kriven and Bischoff [190] observed that the critical grain size for retaining the metastable tetragonal phase in $\text{Hf}_{0.5}\text{Zr}_{0.5}\text{O}_2$ constrained in an alumina matrix was 30 nm. The special fabrication techniques

required to obtain such fine-grained second-phase particles in ceramic matrices usually involve a high production cost.

The third disadvantage in using HfO_2 and $\text{ZrO}_2\text{-HfO}_2$ solid solutions as toughening agents is the reduced stiffness encountered in all matrix materials at 1100–1700 °C. This implies that the level of constraint applied by the matrix material is much reduced and therefore the retained metastable tetragonal phase is less inclined to stress-induced transformation than would be the case for one retained by a matrix with high stiffness [130, 136].

Finally, the natural sources for HfO_2 -based ceramics are much less abundant than those for ZrO_2 , and it is extremely expensive to process a large quantity of high-purity HfO_2 . The high density of HfO_2 ceramics

(9.68–10.30 g cm^{-3} , depending on structural forms retained), Table XI, may also limit their structural applications.

8. Physical properties of HfO_2 -toughened ceramics

A limited amount of published work is available in the literature on the physical and mechanical properties of HfO_2 and HfO_2 -toughened ceramics. Table XII summarises some of the physical properties for HfO_2 ceramics.

8.1. Thermal expansion coefficient

Tables XIII and XIV contain some of the thermal expansion data for HfO_2 ceramics, together with those for ZrO_2 ceramics to enable comparison. Monoclinic (unstabilized) HfO_2 exhibits a strong anisotropy in the thermal expansion coefficient (this is also shown in Fig. 4) [82, 197, 202]. The thermal expansion coefficient of tetragonal HfO_2 (the major constituent phase of partially stabilized HfO_2 ceramics) is also slightly anisotropic. The average values for the thermal expansion coefficients of unstabilized, partially and fully stabilized polycrystalline HfO_2 ceramics follows the order of unstabilized < partially stabilized < fully stabilized. In comparison with those of ZrO_2 ceramics,

TABLE XI The apparent density as a function of composition in $\text{HfO}_2\text{-ZrO}_2$ solid solutions (monoclinic) [189]

Composition $\text{Hf}_{1-x}\text{Zr}_x\text{O}_2$	Apparent density (g cm^{-3})
0.00	9.70
0.04	9.32
0.22	8.27
0.31	8.02
0.51	6.95
0.71	6.40
1.00	5.60

TABLE XII A brief summary of the physical properties of HfO_2 ceramics

Parameters	Value (description)	Reference
Colour	Yellowish white	[47, 48]
Molecular weight	210.49	[32]
Melting point	2900 °C	[30]
Boiling point	4427 °C	[194]
	5400 °C	[195]
Vapour pressure	3×10^{-5} atm (at 2667 °C)	[196]
Index of refraction	1.98–2.02	[15]
Density	9.68 (monoclinic)	[80]
	10.01 (tetragonal)	[80]
	10.30 (cubic)	[15]
Young's modulus	200–250 GPa	[197–200]
Shear modulus	100–110 GPa	[197–200]
Poisson's ratio	0.25–0.30	[197, 198]
Hardness	12–15 GPa	[18, 87]

TABLE XIII The average linear thermal expansion coefficients of unstabilized and stabilized HfO_2 ceramics

Materials composition	Thermal expansion coefficient ($\times 10^{-6}$)	Temperature range (°C)	Reference
HfO_2	4.4	25–1000	[201]
HfO_2	4.7		[174]
$\text{HfO}_2\text{-10 wt \% Y}_2\text{O}_3$	6.33	25–2500	[191]
$\text{HfO}_2\text{-15 wt \% Y}_2\text{O}_3$	6.27		[191]
$\text{HfO}_2\text{-3 mol \% Er}_2\text{O}_3$	6.5	25–1700	[174]
$\text{HfO}_2\text{-5 mol \% Er}_2\text{O}_3$	7.1		[174]
$\text{HfO}_2\text{-9 mol \% Er}_2\text{O}_3$	7.2		[174]
HfO_2 (Er_2O_3 FSZ)	9.4		[174]
$\text{HfO}_2\text{-2 mol \% Yb}_2\text{O}_3$	5.3	25–1750	[109]
$\text{HfO}_2\text{-6 mol \% Yb}_2\text{O}_3$	7.5		[109]
HfO_2 (Yb_2O_3 FSZ)	8.5		[109]
ZrO_2	7.6–10	25–1000	[201]
ZrO_2 (PSZ)	8–11		[38]
ZrO_2 (FSZ)	10–13		[38]

PSZ, partially stabilized zirconia; FSZ, fully stabilized zirconia.

TABLE XIV Average axial and volume thermal expansion coefficients for monoclinic and tetragonal HfO₂ ceramics. The relevant data for ZrO₂ ceramics are included for comparison

Phases	Average axial thermal expansion coefficients ($\times 10^{-6}$)					Temperature range ($^{\circ}$)	Reference
	<i>a</i>	<i>b</i>	<i>c</i>	β	<i>V</i>		
Mono. HfO ₂	6.1	0.0	9.6	3.6	20.6		[49]
	7.4	0.06	12.2		20.6	25–1000	[201]
	7.5	1.4	11.9		20.8	25–1000	[104]
	8.4	2.7	11.3		23.5	25–1000	[105]
	7.2	1.5	12.6		23.0	25–1000	[106]
	7.6	1.2	11.2		21.6	25–1000	[81]
Mono. ZrO ₂	9.2	1.4	10.9		22.9	25–1000	[201]
	7.8	1.5	12.8		23.1		[104]
	8.3	1.9	13.5		25.9		[105]
	9.2	0.6	14.2		28.0		[106]
Tetra. HfO ₂	6.1		5.6		37.2		[49]
Tetra. ZrO ₂	7.9		6.2				[82]

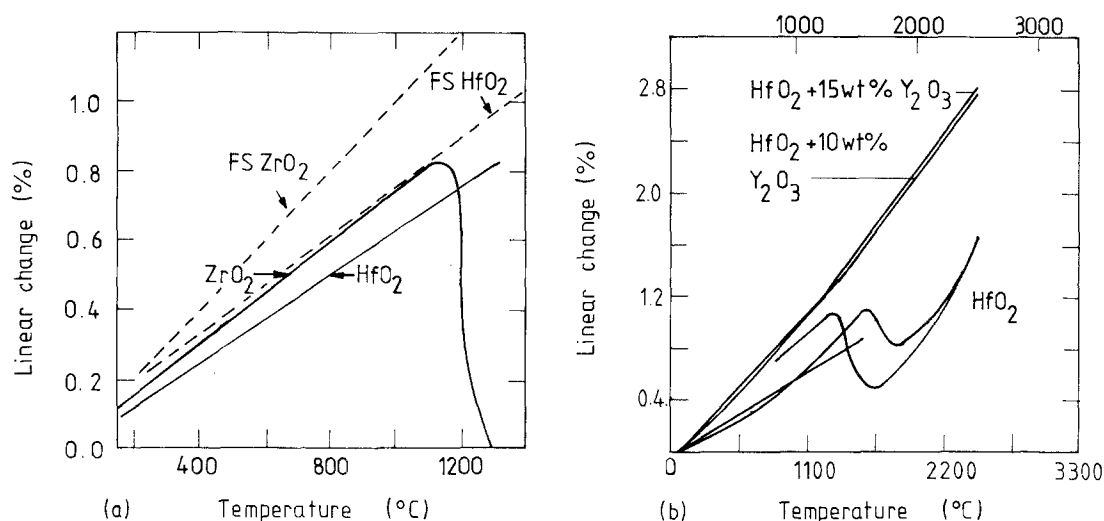


Figure 22 (a, b) The thermal expansion (linear percentage) of unstabilized and fully stabilized (Y₂O₃ and CaO) HfO₂ and ZrO₂ ceramics as a function of temperature [80, 191]. FS refers to CaO fully stabilized.

the average thermal expansion coefficients of HfO₂ ceramics are slightly lower.

Fig. 22a and b are examples showing the linear thermal expansion of HfO₂ ceramics as a function of temperature. The results for ZrO₂ ceramics are also included. The curves for unstabilized HfO₂ and Y₂O₃ fully stabilized HfO₂ were obtained by Ohnysty and Rose [191] and those for CaO-stabilized HfO₂ and ZrO₂ by Curtis *et al.* [80]. The polymorphism and the monoclinic \rightleftharpoons tetragonal transformations in the unstabilized HfO₂ are clearly indicated by the thermal expansion curve as a sharp change in the dimension of the specimen in the temperature range 1600–1800 °C. In contrast, Y₂O₃-stabilized HfO₂ shows a continuous (and slightly above that for the unstabilized HfO₂) thermal expansion curve from room temperature to above the monoclinic to tetragonal transformation temperature. This continuity indicates that there are no phase transformations nor any substantial structural changes occurring in this temperature range.

As was discussed in Section 6.3.9, a continuous solid solution occurs in the HfO₂–ZrO₂ system. Thermal expansion of HfO₂–ZrO₂ solid solution was observed to follow approximately the rule of mixtures,

decreasing almost linearly with increasing HfO₂ content, Table X.

8.2. Elastic properties

Elastic properties of HfO₂-based materials are dependent on temperature and microstructural parameters such as porosity level, grain size, and the phases present in the sintered bodies [203, 204]. For unstabilized HfO₂ ceramics, the elastic properties may also show a sudden change at the monoclinic \rightleftharpoons tetragonal transformation temperatures [205, 206]. Table XV is a brief summary of the elastic properties for HfO₂ ceramics.

As with most other engineering ceramics, the elastic properties of HfO₂ based ceramics deteriorate with increasing temperature. Fig. 23 is an example showing the relative Young's modulus for polycrystalline HfO₂ ceramics containing 20 mol % Y₂O₃ and 20 mol % Er₂O₃, respectively, as a function of temperature. It illustrates a non-linear relationship [198]. From room temperature to 500 °C, the Young's modulus decreases non-linearly, at an average rate of 3%/100 °C and from 500–1000 °C at an average rate of 1%/100 °C. It

TABLE XV A Summary of the elastic properties of HfO₂-based ceramics

Composition	E^a (GPa)	G^a (GPa)	B^a (GPa)	ν^a	Reference
Unstabilized polycrystals	283.6	109.2	233.1	0.2984	[199]
PSH polycrystals (7.6 mol % Y ₂ O ₃)	253.3	101.9		0.2430	[197]
FSH polycrystals (12 mol % Y ₂ O ₃)	246.0			0.2740	[18, 87]
FSH polycrystals (20 mol % Er ₂ O ₃)	246.0			0.2740	[198, 207]
FSH polycrystals (33 mol % Pr ₂ O ₃)	238.2	93.2			[207]
FSH single crystal (12 mol % Y ₂ O ₃)	C_{11} 380	C_{12} 90	C_{44} 80		[18, 87]

^a E , G , B , and ν are Young's modulus, shear modulus, bulk modulus, and Poisson's ratio, respectively. FSH, fully stabilized hafnia.

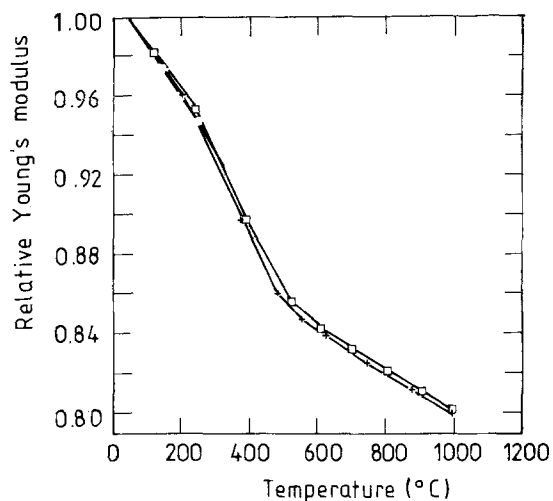


Figure 23 The relative Young's modulus as a function of temperature for (+) Y₂O₃ (20 mol %) and (□) Er₂O₃ (20 mol %) stabilized HfO₂ ceramics [198], indicating a non-linear relationship.

was further observed that the elastic modulus decreased rapidly at temperatures above 1000 °C. The non-linear behaviour was affected by the type and amount of alloying oxides. It was therefore proposed that oxygen-vacancy motion was one of the possible mechanisms behind such non-linear behaviour [198].

For unstabilized polycrystalline HfO₂ ceramics, the most important microstructural parameter found to affect the elastic properties was the porosity level present in the sintered structure. On the basis of their experimental results, Figs 24 a, b and 25a, b, Dole *et al.* [199] found their data to fit the following equations

$$E = 283.6 \exp(-4.17 P_p) \text{ (GPa)} \quad (12)$$

$$G = 109.2 \exp(-3.93 P_p) \text{ (GPa)} \quad (13)$$

$$B = 233.1 \exp(-5.48 P_p) \text{ (GPa)} \quad (14)$$

where E , G , and B are the Young's modulus, shear modulus, and bulk modulus, respectively. P_p is the percentage porosity found in the sintered materials. It is apparent that the zero porosity values for the elastic modulus, shear modulus, and bulk modulus are 283.6, 109.2 and 233.1 GPa, respectively. These values are very close to those reported for unstabilized ZrO₂ ceramics [38]. The Poisson's ratio for zero-porosity

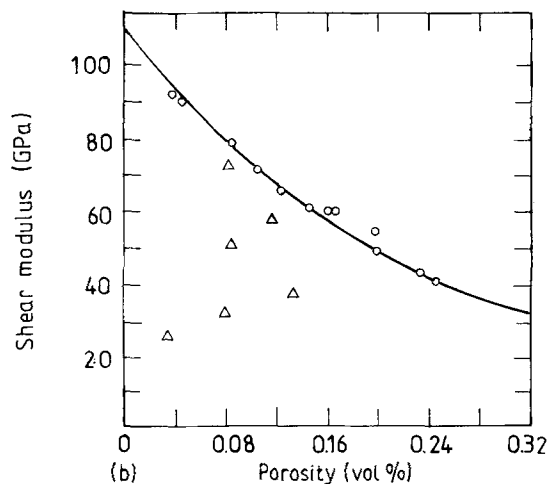
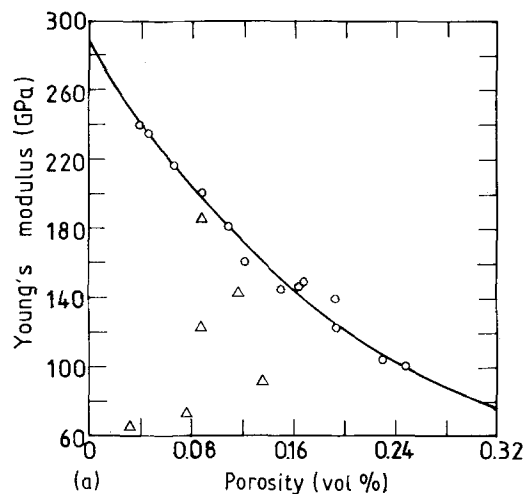


Figure 24 (a) Young's modulus and (b) shear modulus of unstabilized HfO₂ ceramics as a function of volume fraction porosity [199]. The presence of microcracks (Δ), which is a result of the tetragonal to monoclinic transformation and/or the anisotropic thermal expansion of monoclinic HfO₂ grains, has a much more devastating effect on reducing the elastic constants of polycrystalline HfO₂ ceramics than does the same amount of porosity (○).

unstabilized HfO₂ is 0.2984, as calculated by Dole *et al.* [199, 222].

It has been observed that the presence of microcracks, which is a result of the volume expansion and shear strain associated the tetragonal to monoclinic transformation or/and the anisotropic thermal expansion of monoclinic phase, in unstabilized HfO₂

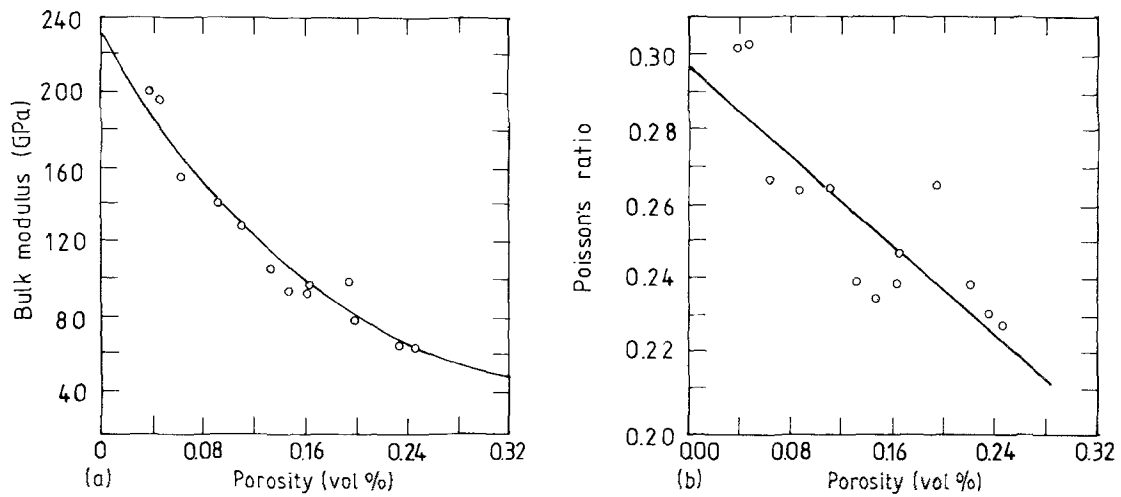


Figure 25 (a) Bulk modulus and (b) Poisson's ratio of unstabilized HfO_2 as a function of volume fraction porosity [199].

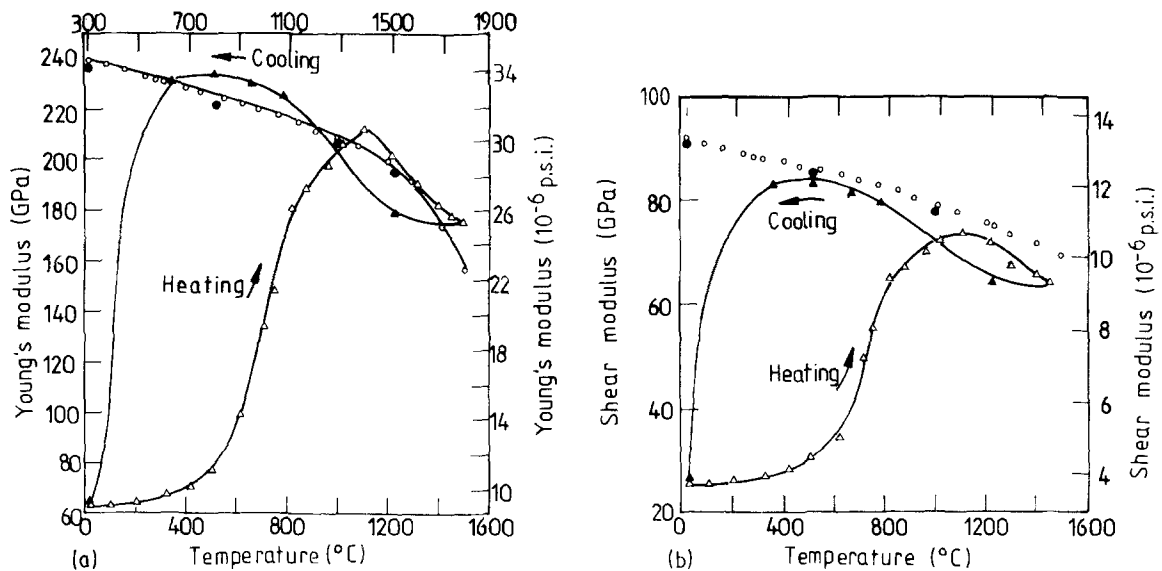


Figure 26 (a) Young's modulus and (b) shear modulus as a function of temperature for (Δ) a microcracked (unstabilized) and (\circ) crack-free (fully stabilized) HfO_2 ceramic [198, 199]. The fully stabilized specimen shows a continuous decrease both in Young's modulus and in shear modulus with increasing temperature. In contrast, the microcracked specimen exhibits a well-defined hysteresis loop after each heating and cooling cycle (solid symbols).

ceramics results in a much more devastating reduction in the elasticity than does the same amount of porosity, Fig. 24a and b. This phenomenon is related to the effect of pore shape on the elasticity of polycrystalline ceramics [208].

A similar study was carried out by Scheidecker [197] and Dole [200] on partially stabilized HfO_2 ceramics, which were doped with Er_2O_3 (4.4 mol %), Y_2O_3 (7.6 mol %), and Eu_2O_3 (4.1 mol %), respectively. The presence of porosity in these partially stabilized HfO_2 ceramics results in a similar decrease in the elastic constants as it does to the unstabilized HfO_2 ceramics discussed above. The zero porosity Young's, shear, and bulk moduli for these partially stabilized HfO_2 ceramics were shown to be close to 250.0, 100.0 and 160.0 GPa, respectively. These values are lower than those for the unstabilized HfO_2 ceramics. Their Poisson's ratio, close to 0.2430, is also lower than that for unstabilized HfO_2 ceramics.

The second important microstructural parameter that needs to be considered as influencing elastic

properties of unstabilized HfO_2 ceramics is the grain size. It was shown that there existed a critical grain size at which a drastic reduction in the elastic properties occurred [198–200]. The grain size dependence of the elastic properties can be interpreted in terms of the observation that the residual strain energy resulting from thermal expansion anisotropy of unstabilized HfO_2 grains causes microcracks at a sufficient large grain size, on cooling from the sintering temperature. It was shown that the critical grain size for spontaneous microcracks in unstabilized HfO_2 was $\sim 2.0 \mu\text{m}$ [198, 199]. As mentioned above, the presence of microcracks due to the anisotropic thermal expansion resulted in a much more drastic reduction in the elastic properties than was caused by the same amount of porosity.

Moreover, the microcracks associated with the anisotropic thermal expansion strongly affect the temperature dependence of the elastic properties in unstabilized HfO_2 ceramics [198, 199, 221]. Fig. 26a and b show the Young's modulus and shear modulus,

respectively, as a function of temperature for an unstabilized and fully stabilized HfO₂. They have a similar relative density (96.5% theoretical density). The fully stabilized specimen shows a continuous decrease in the elastic moduli with increasing temperature, typical of polycrystalline ceramics [208]. The moduli also retrace their heating paths during cooling, indicating that significant microstructural change has not occurred after the thermal cycling.

In comparison, the unstabilized HfO₂ specimen, which has a grain size of 16 μm [198, 199], exhibits a much lower Young's modulus (16%) than that of the fully stabilized specimen, even though their sintered densities are close to each other, Fig. 26a. The heating and cooling moduli form a distinct hysteresis loop, a characteristic which has been observed in many other microcracked ceramics. When the specimen is heated, the modulus shows a continuous increase up to 1100 °C with a maximum rate at 800 °C. At temperatures > 1100 °C, it approaches close to and follows the value for the fully stabilized specimen. When cooled, it traces the path for the stabilized specimen down to 400 °C, where it starts to decrease more rapidly to the value at room temperature before the thermal cycling. As is shown in Fig. 26b, the heating and cooling shear moduli also form a distinct hysteresis loop.

Such hysteresis behaviour for unstabilized HfO₂ ceramics can best be explained by a microcrack healing and formation process, in which thermal energy facilitates microcrack healing during heating and the thermal expansion anisotropy-induced microstress causes microcracks to form during cooling. The microcrack healing and formation process is affected by experimental conditions such as the heating and cooling rates, number of thermal cycles, and the atmosphere experienced by the specimen [208].

The Young's modulus and Poisson's ratio for fully stabilized HfO₂ single crystal are 246 GPa and 0.274, respectively, as determined by Ingel *et al.* [87] for the composition containing 12 mol % Y₂O₃ (210 GPa and 0.307 were measured for a ZrO₂ single crystal containing the same amount of Y₂O₃). These values can be regarded as an approximation for the zero porosity elastic constants of fully stabilized polycrystalline HfO₂ ceramics.

8.3. Hardness

Not surprisingly, the hardness value for unstabilized polycrystalline HfO₂ ceramics is not available in published work. Sintered HfO₂ ceramics, as such, are not considered to be a class of hard materials, as they almost always contain a considerably high level of porosity and/or microcracks. The hardness values for partially and fully stabilized HfO₂ single crystals obtained by Rice and co-workers [18, 87] are shown in Fig. 27, together with those for partially and fully stabilized ZrO₂ single crystals for comparison. The hardness of HfO₂ single crystal increases steadily with increasing Y₂O₃ content in the composition range 3–6 mol % Y₂O₃, and remains almost unchanged with further increase in Y₂O₃ content in the composi-

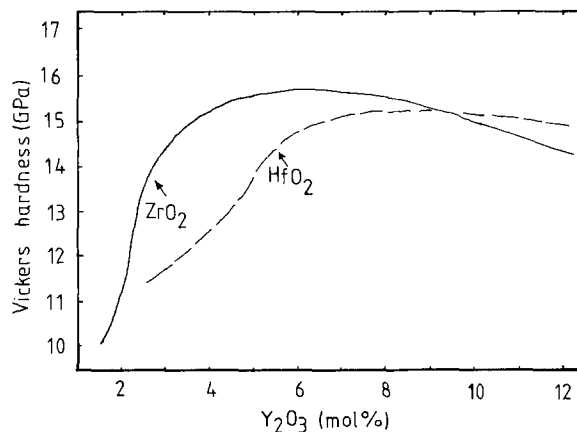


Figure 27 The dependence of hardness on Y₂O₃ content for HfO₂ and ZrO₂ single crystals, grown using skull melting technique by Rice *et al.* [18]. The hardness increases sharply from 2.0–3.0 mol % Y₂O₃ for ZrO₂ and from 3–6 mol % Y₂O₃ for HfO₂.

tion range 6–10 mol % Y₂O₃. ZrO₂ single crystal exhibits similar behaviour, but a sharp increase in hardness occurs in the composition range 2–3 mol % Y₂O₃. These results are representative of hardness values for partially and fully stabilized polycrystalline HfO₂ ceramics, whose hardness will be strongly influenced by their microstructural and composition parameters, such as the porosity level and grain size. For example, it was observed that the hardness of fully stabilized polycrystalline HfO₂ ceramics decreased with increasing alloying oxide content [209]. For a fixed amount of alloying content, it was also affected by the type of alloying oxides; Er₂O₃-stabilized HfO₂ always exhibits a hardness value exceeding that for the Sc₂O₃-stabilized material. It was suggested that such phenomenon was related to the defect concentrations of anion sublattices and anion-vacancy orderings in the stabilized HfO₂.

9. Fracture strength and fracture toughness

9.1. Unstabilized HfO₂

Although the relationships between mechanical properties and microstructure are not well established for unstabilized HfO₂ ceramics, as such, they are not regarded as a class of potentially important structural ceramics for mechanical purposes. This is due to the low sintered density and the presence of microcracks, and consequently the poor mechanical properties. As an example, Staszak [49] quoted a fracture strength of 200 MPa and a fracture toughness of 2.0 MPa m^{0.5} for unstabilized HfO₂ ceramics. Generally, undoped HfO₂ ceramics are fabricated via the conventional sintering or hot pressing of commercially available HfO₂ powders. The fact that unstabilized HfO₂ exhibits a monoclinic structure may partially explain why it is so difficult to achieve a high sintered density via pressureless sintering. It is likely that there exists a network of microcracks in the sintered structures, induced by the anisotropic thermal expansion and the volume expansion and shear strain associated with the tetragonal to monoclinic transformation on cooling from the sintering temperature. The formation of these

microcracks results in a reduction in the sintered density and therefore the mechanical properties of unstabilized HfO₂ ceramics. For those sintered at temperatures < 1720 °C (below the monoclinic to tetragonal transformation temperature), the microcracks are a result of the anisotropic thermal expansion of the monoclinic phase, see Table XIV, which generates residual stresses on cooling from the sintering temperature. For those sintered at temperatures > 1720 °C, both the volume expansion and shear strain associated with the tetragonal to monoclinic transformation and the subsequent anisotropic thermal expansion of monoclinic phase cause serious cracking.

9.2. Partially stabilized HfO₂ ceramics

The development of partially stabilized HfO₂ ceramics in the late 1970s and the early 1980s was encouraged by the results obtained on the transformation-toughened ceramics of the ZrO₂-based systems [1–6]. It was expected that similarly toughened ceramics could be fabricated in the HfO₂-based systems, particularly when one considered the structural similarity that is found between HfO₂ and ZrO₂. However, a less than successful story has evolved in the case of the HfO₂-toughened ceramics. This has been in spite of the identical fabrication routes being employed and the same alloying oxides, namely, Y₂O₃, CeO₂ and Er₂O₃, being used to partially stabilize HfO₂.

As is expected, the mechanical properties of partially stabilized HfO₂ ceramics are largely dependent on the amount of metastable tetragonal phase retained in their structures [122, 210]. It is therefore important to control the amount of alloying oxide added and the grain size of the sintered materials, because they are the two parameters most influential in retaining the metastable tetragonal phase. Unfortunately, the precise values for these parameters are not well established in each of the HfO₂-based systems. Moreover, tetragonal hafnia polycrystals (THPs) have never been obtained in any HfO₂-based systems. This is very different from the situation in the ZrO₂-based ceramic systems, among which tetragonal zirconia polycrystals (TZPs) are readily obtainable in the Y₂O₃- and CeO₂-ZrO₂ systems [147]. A brief survey

of the partially stabilized HfO₂ ceramics which have been fabricated, is now given, the mechanical properties of which are closely related to the amount of metastable tetragonal phase retained and their microstructure.

The fracture toughness obtained by Ingel *et al.* [87] for a partially stabilized HfO₂ single crystal containing 4.5 mol % Y₂O₃ was 4.1 MPa m^{0.5}, compared with 3.0 for a ZrO₂ single crystal containing the same amount of Y₂O₃. The dependence of fracture toughness on Y₂O₃ content for partially stabilized HfO₂ single crystals, which were grown using the skull melting technique, is shown in Fig. 28 [18]. The results for ZrO₂ single crystals prepared using the same technique are included for comparison. The fracture toughness appears to increase with increasing Y₂O₃ content from 3.0 mol % to 4 mol %, where a maximum toughness value of 4.6 MPa m^{0.5} is reached. With a further increase in the Y₂O₃ content, the fracture toughness shows a continuous decrease. Although the ZrO₂ single crystals exhibit similar behaviour, two apparent differences are:

- (i) the peak fracture toughness (~ 8.2 MPa m^{0.5}) is much higher than that for the HfO₂ single crystal;
- (ii) the fracture toughness is maximized at 2 mol % Y₂O₃, instead of at 4 mol % Y₂O₃.

It is thus apparent that a higher Y₂O₃ content is required to stabilize HfO₂ ceramics than to stabilize ZrO₂ ceramics for a maximum toughness. Conversely, an HfO₂ ceramic may exhibit a much lower degree of stabilization than a ZrO₂ ceramic containing the same amount of Y₂O₃. As is shown in Fig. 28, 3 mol % Y₂O₃ results in an under-stabilization and an over-stabilization for HfO₂ and ZrO₂, respectively. It was observed using TEM that both the density and size of the tetragonal/monoclinic precipitates in the HfO₂ single crystal containing 4.5 mol % Y₂O₃ are greater than those in the ZrO₂ single crystal containing the same amount of Y₂O₃, indicating that a higher degree of stabilization is achieved in the latter than in the former [32, 133].

Y₂O₃ partially stabilized polycrystalline HfO₂ ceramics were fabricated by Ikuma and Virkar [211] in their study of the crack-size dependence of fracture toughness in transformation-toughened ceramics. HfO₂ and Y₂O₃ powders were mechanically mixed

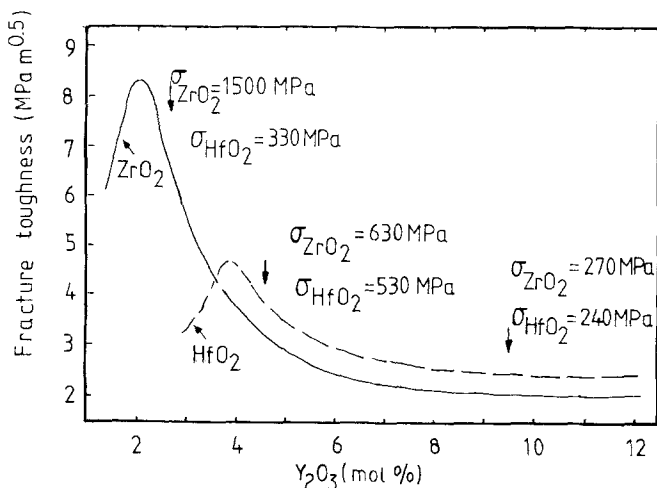


Figure 28 The dependence of fracture toughness on Y₂O₃ content for HfO₂ and ZrO₂ single crystals, grown using the skull melting technique by Rice *et al.* [18]. The strength data are for the compositions indicated.

together in a ball mill to obtain a composition of HfO_2 -5.5 mol % Y_2O_3 . The sintered specimen was expected to consist of tetragonal (probably precipitates) and cubic phases, although the authors failed to report the exact amount of tetragonal phase. The fracture toughness measured in the sintered specimen was in the range 4–6 $\text{MPa m}^{0.5}$, increasing with increasing crack length (controlled by the indentation load). It is therefore to be concluded that stress-induced transformation toughening is occurring in this partially stabilized polycrystalline HfO_2 ceramic.

A comprehensive study on Er_2O_3 partially stabilized HfO_2 was made by Hunter and co-workers [67, 122, 210]. They investigated both the conditions for retaining the metastable tetragonal phase in terms of grain size and Er_2O_3 alloying content, together with the mechanical properties of the Er_2O_3 partially stabilized HfO_2 ceramics. Firstly, it was observed that the critical grain size for retaining the metastable tetragonal phase was extremely small for unstabilized HfO_2 , 4–10 nm. The critical grain size, < 50 nm, for 1 mol % Er_2O_3 partially stabilized HfO_2 was also found difficult to obtain via a conventional ceramic fabrication process, such as the sintering of mixed oxide powder compacts.

In order to obtain a fine grain sized material, Hunter *et al.* [67, 122] employed the following experimental route to fabricate the Er_2O_3 partially stabilized HfO_2 . Acid solutions of $\text{Er}(\text{NO}_3)_3$ and $\text{Hf}(\text{NO}_3)_4$ were mixed together to obtain a composition of 1 mol % Er_2O_3 -doped HfO_2 , and Hf-Er hydroxide was co-precipitated out with dilute ammonia solution. The hydroxide was washed with water initially and subsequently was further washed with acetone and toluene to obtain an active fast-drying powder. The dried powder was then calcined either at 1150 °C for 4 h or at 600 °C for 15 h to yield the desired oxide powder. The densified specimens were obtained by vacuum hot pressing in a graphite die at temperatures of 1500–1650 °C and at pressures of up to 150 MPa. The fracture toughness, K_{IC} , and the fracture energy, γ , were determined by the notched beam bar test.

Fig. 29 shows the fracture toughness, K_{IC} , and Fig. 30 shows the fracture energy, γ , of the Er_2O_3 partially stabilized HfO_2 ceramics, as a function of the amount of metastable tetragonal phase retained in the structure, as determined by X-ray diffraction analysis. The fracture toughness shows a general increase as increasing amounts of tetragonal phase retained, whereas the fracture energy shows a small increase until the fraction of tetragonal phase reaches about 20%, where there is a significant increase. Hunter *et al.* [67, 122] also mentioned that one of their specimens contained 46% metastable tetragonal phase, which was the highest amount of tetragonal phase retained in partially stabilized HfO_2 ceramics ever reported in published work. However they were unable to reproduce this result.

9.3. Fully stabilized HfO_2 ceramics

The fracture strength and fracture toughness, which are dependent on microstructural parameters such as

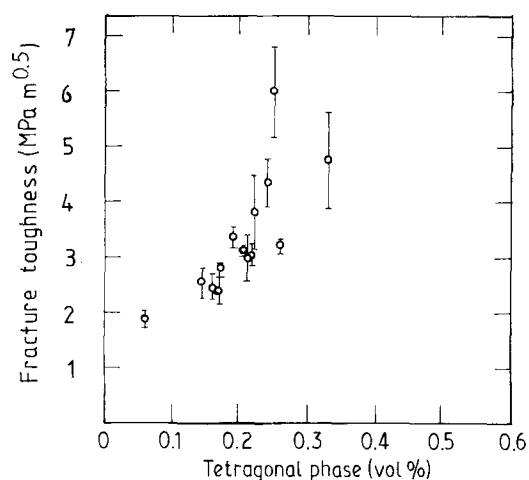


Figure 29 The fracture toughness as a function of tetragonal phase content in Er_2O_3 partially stabilized hafnia ceramics [67, 122].

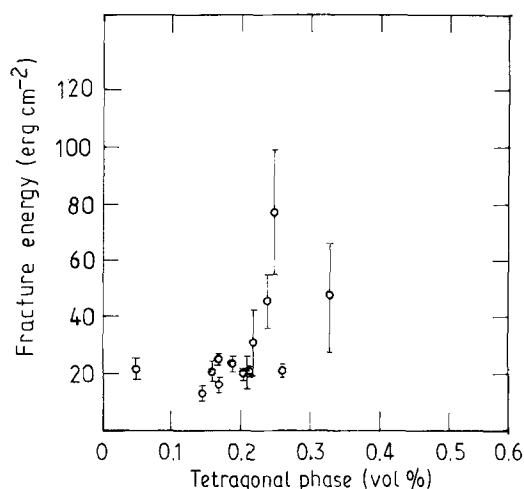


Figure 30 The fracture energy of Er_2O_3 partially stabilized HfO_2 ceramics as a function of tetragonal phase retained [67, 122].

grain size and porosity level, of fully stabilized HfO_2 ceramics are considered to be similar to those of fully stabilized polycrystalline ZrO_2 ceramics, ranging from 200–300 MPa and from 2–3 $\text{MPa m}^{0.5}$, respectively [209, 210, 212]. For example, an indentation toughness of 2.0 $\text{MPa m}^{0.5}$ was measured both for a fully stabilized HfO_2 single crystal containing 12 mol % Y_2O_3 [87] and for a fully stabilized polycrystalline ZrO_2 ceramic containing the same amount of Y_2O_3 [211]. A flexural strength of 240 MPa for a HfO_2 single crystal containing 9.5 mol % Y_2O_3 was obtained, compared with 270 MPa for a ZrO_2 single crystal containing the same amount of Y_2O_3 [18].

9.4. HfO_2 -toughened Al_2O_3 ceramics

Although hafnia-toughened alumina (HTA) ceramics were recognized similar to zirconia-toughened alumina (ZTA) ceramics more than one decade ago by Claussen and co-workers [4, 5, 193, 213], only a limited amount of research work has since been undertaken to investigate their fabrication, microstructure and mechanical properties. A recent study was due to Wang and Stevens [214], who fabricated HTA ceramics containing 5–30 vol % HfO_2 in Al_2O_3 matrices via

conventional sintering of mixed Al_2O_3 and HfO_2 powders at 1625°C . The sintered specimens were then subjected to thermal treatments at 1750°C for 0.5 h and 1600°C for 5 h, respectively. It was shown that the microstructure and therefore the mechanical properties of these materials were dependent on the thermal treatment procedures. A fracture toughness of $5.5 \text{ MPa m}^{0.5}$ and a fracture strength of $\sim 400 \text{ MPa}$ were measured for the as-sintered specimen containing 15 vol % HfO_2 , compared with a fracture toughness of $\sim 8.0 \text{ MPa m}^{0.5}$ and a fracture strength of $\sim 250 \text{ MPa}$ for the specimen subjected to the further thermal treatment at 1750°C for 0.5 h. A well-distributed microcrack network was developed in the further treated material, as 1750°C was above the monoclinic to tetragonal transformation temperature of HfO_2 . Therefore the volume expansion and shear strain associated with the tetragonal to monoclinic transformation of HfO_2 inclusions resulted in the formation of a microcrack network, which was responsible for the improved fracture toughness. However, if the microcracked specimen was thermally treated at 1600°C for 5 h, the microcracks would be healed, as in the case of Al_2O_3 ceramics [215]. The microcrack healing associated with the thermal treatment at 1600°C for 5 h was indicated by the reduced fracture toughness ($\sim 4.5 \text{ MPa m}^{0.5}$) and the partially recovered fracture strength ($\sim 350 \text{ MPa}$).

The thermal and mechanical properties of HTA ceramics can be further modified by the introduction of other oxides. A well-published example is that of the transformation toughened ceramics in the Al_2O_3 - Cr_2O_3 / ZrO_2 - HfO_2 system, which has been extensively exploited by Brog and co-workers [139, 140, 216]. They considered that these toughened ceramics were potential candidate materials for heat engine applications and therefore aimed to reduce their thermal conductivity and to improve their high-temperature performance. The materials they investigated were fabricated by the hot pressing of mixed pre-reacted Al_2O_3 - Cr_2O_3 and ZrO_2 - HfO_2 powders at $1500^\circ\text{C}/35 \text{ MPa}$ in a boron nitride-coated graphite

die, heated by a graphite resistance furnace. The thermal and mechanical property measurements were subsequently carried out on the hot-pressed specimens. Microstructurally, the hot-pressed materials consisted of an Al_2O_3 - Cr_2O_3 matrix and well-dispersed ZrO_2 - HfO_2 solid solution inclusions. The tetragonal phase retained in the dispersed ZrO_2 - HfO_2 solid solution inclusions decreased with increasing HfO_2 alloying from 10–30 mol %.

It was observed that the Cr_2O_3 alloying in the Al_2O_3 matrix significantly reduced the thermal conductivity of the HfO_2 toughened Al_2O_3 , as measured by the “laser flash” method. The elastic modulus, as determined using the sonic method, obeyed approximately the rule of mixture, i.e. decreased as the amount of dispersed phase increased. For composites containing the same amount of dispersed phase, the specimen containing 30 mol % HfO_2 in the dispersed phase had a higher elastic modulus than did those containing 10 mol % HfO_2 .

The fracture strength of these composites was dependent both on the amount of dispersed ZrO_2 - HfO_2 solid solution in Al_2O_3 - Cr_2O_3 matrix and on the degree of HfO_2 alloying in the dispersed phase, Fig. 31. At high inclusion loading, the specimen containing 30 mol % HfO_2 in the dispersed phase exhibited a greater fracture strength than the specimen containing 10 mol % HfO_2 . These results, together with those of elastic property measurement, suggested that the former contained a lower density of microcracks than the latter. This can be interpreted on the basis that the volume change and shear strain associated with the tetragonal to monoclinic transformation decreases with increasing HfO_2 alloying content in the solid solution.

The fracture toughness, as determined by the indentation and bend strength techniques, increased initially as a function of volume fraction of the dispersed ZrO_2 - HfO_2 solid solution and declined after reaching a maximum, Fig. 32. The reduced fracture toughness at high loadings of the dispersed solid solution can be accounted for by the decreased amount of tetragonal phase retained in the matrix. It was further shown that the thermal stability of these composites was substantially higher than conventional zirconia toughened alumina (ZTA) ceramics, as indicated by the observation that no degradation in density, elastic modulus, bend strength and fracture toughness was shown after they were held at 1000°C for more than 500 h. However, further investigation is needed in order to understand fully the mechanisms behind this improved thermal stability, i.e. was it due to the Cr_2O_3 solid solution in the Al_2O_3 matrix or the HfO_2 alloying in the dispersed phase?

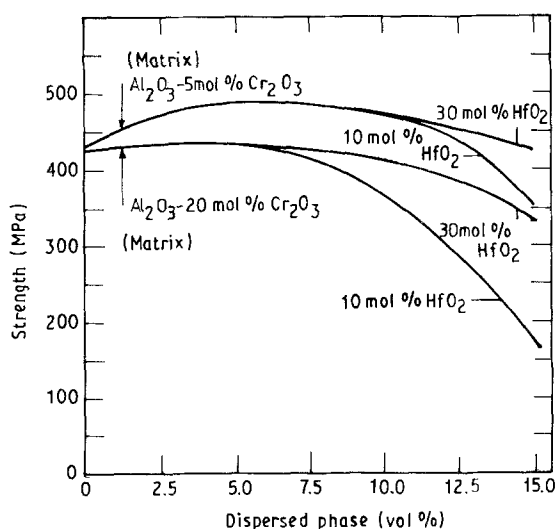


Figure 31 The bend strength of HfO_2 - ZrO_2 solid solution toughened Al_2O_3 - Cr_2O_3 ceramics as a function of volume fraction of the dispersed phase [139].

9.5. HfO_2 -toughened Si_3N_4 ceramics

In a US Patent, Carpenter [217] described the fabrication and mechanical properties of HfO_2 -based oxide toughened Si_3N_4 composite ceramics. The composites consist of a Si_3N_4 matrix and inclusions of ternary HfO_2 - ZrO_2 - TiO_2 solid solution, which contains 60–85 mol % HfO_2 , 10–30 mol % ZrO_2 , and 10–30

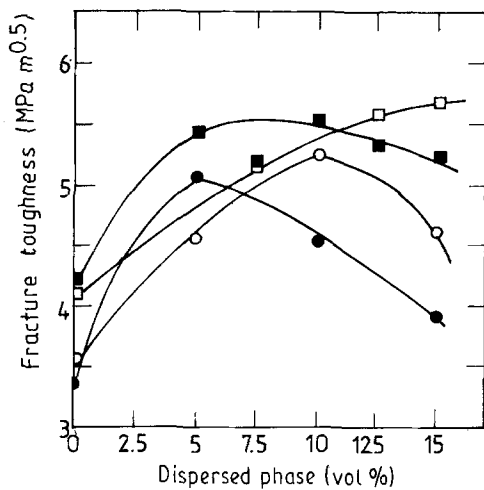


Figure 32 The fracture toughness of the $\text{Al}_2\text{O}_3\text{-Cr}_2\text{O}_3/\text{HfO}_2\text{-ZrO}_2$ composites as a function of volume fraction of the dispersed $\text{HfO}_2\text{-ZrO}_2$ phase [139]. (O) $\text{Al}_2\text{O}_3\text{-20 mol \% Cr}_2\text{O}_3/\text{ZrO}_2\text{-10 mol \% HfO}_2$. (●) $\text{Al}_2\text{O}_3\text{-20 mol \% Cr}_2\text{O}_3/\text{ZrO}_2\text{-30 mol \% HfO}_2$. (□) $\text{Al}_2\text{O}_3\text{-5 mol \% Cr}_2\text{O}_3/\text{ZrO}_2\text{-10 mol \% HfO}_2$. (■) $\text{Al}_2\text{O}_3\text{-5 mol \% Cr}_2\text{O}_3/\text{ZrO}_2\text{-30 mol \% HfO}_2$.

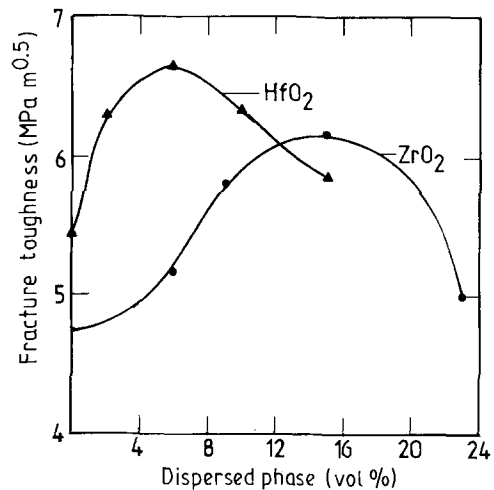


Figure 33 The fracture toughness as a function of HfO_2 content for the SiC/HfO_2 composites [219]. The results for the SiC/ZrO_2 composites fabricated by the same authors are included for comparison.

mol % TiO_2 . They can be prepared via several different fabrication routes, including conventional sintering or hot pressing of mixed pre-reacted oxides and submicrometre Si_3N_4 powders. As an example, the following is one of the most conventional routes which can be employed:

- (i) pre-mixing of the ternary oxides, followed by a calcination to obtain a uniformly mixed solid solution;
- (ii) the ternary oxide solid solution is then milled and subsequently mixed with submicrometre fine Si_3N_4 powder;
- (iii) the mixed composition is then compacted by die pressing and/or isostatic pressing;
- (iv) finally, the green compacts are sintered, or alternatively hot pressed at temperatures of 1600–1700 °C.

The sintered materials exhibit a relative density > 98% theoretical density, a fracture strength of 650 MPa and a fracture toughness of 6–8 $\text{MPa m}^{0.5}$.

9.6. HfO_2 -toughened SiC ceramics

The current structural applications of SiC-based ceramics are related to their potentially desirable thermal and mechanical properties, such as fracture strength, hardness, thermal conductivity and expansion coefficient, and their thermal and chemical stabilities. Technologically, it is desirable to improve the fracture toughness of SiC-based materials in order to widen their applications at both low and high temperatures. However, if one considers transformation toughening as an option for this, two difficulties involved in the fabrication process become apparent, notably low densification rate and the possible reactions between the oxide and the carbide [218]. Therefore, certain special fabrication techniques are required for achieving a high sintered density and suppressing the possible reactions.

Gauckler *et al.* [219] first fabricated SiC/HfO_2 composites via hot isostatic pressing (HIPing) of mixed SiC and HfO_2 powders, together with

5–10 wt % of $\text{Al}_2\text{O}_3 + \text{SiO}_2/\text{mullite}$, as a sintering aid. The purpose of such a small amount of silicate, which melts at < 1700 °C, was two-fold: promoting the densification and suppressing the potential reactions between SiC and HfO_2 grains via the formation of a thin liquid-phase film at the grain boundaries and junctions. As a result, a high sintered density (almost theoretical density) was obtained for the SiC-HfO_2 composites. These authors also fabricated SiC/ZrO_2 composites using the identical processing route.

Fig. 33 shows the fracture toughness of HfO_2 -toughened SiC ceramics fabricated by these authors as a function of HfO_2 addition. Their results for ZrO_2 toughened SiC ceramics are included in Fig. 28 for comparison. It can be seen that the fracture toughness initially increases with increasing HfO_2 addition at low HfO_2 loading. A maximum in the fracture toughness was then obtained when 6 vol % HfO_2 was introduced, followed by a steady decrease with further increasing HfO_2 addition. The ZrO_2 toughened SiC ceramics show a similar behaviour. However, the maximum in fracture toughness was obtained at 15 vol %. Unfortunately, the authors did not give a proper explanation as to how the fracture toughness was improved for the compositions containing < 6 vol % HfO_2 . It is to be expected that crack deflection and residual stresses may well play an important role in determining the mechanical properties of these materials. Transformation toughening is not to be expected as the tetragonal HfO_2 phase was not present in the hot-pressed composites.

10. Conclusions

A review has been made of the science and technology of HfO_2 -based and HfO_2 -containing ceramics. Although HfO_2 ceramics are very similar to ZrO_2 ceramics in many respects, they are considerably different in terms of their transformation toughening behaviour. The potential for HfO_2 ceramics to generate much improved mechanical properties over ZrO_2 ceramics has not been revealed in the published work.

The improvement in mechanical properties associated with the tetragonal to monoclinic transformation in HfO_2 is, in fact, less than that associated with ZrO_2 , due to the fact that the effective volume expansion associated with the transformation in the former is smaller than in the latter. The retention of metastable tetragonal HfO_2 phase, which is vital in determining the mechanical property improvement associated with transformation toughening, is much more difficult to achieve than is the retention of metastable ZrO_2 phase in a ceramic matrix. This is a consequence of the much reduced critical grain size for the spontaneous tetragonal to monoclinic transformation in HfO_2 . Further investigation is needed to confirm whether a fine enough grain size will result in the retention of a high volume fraction of metastable tetragonal HfO_2 phase in ceramic matrices and the mechanical properties to be expected.

Acknowledgement

The authors wish to thank Dr C. G. Neeson, IRC in Materials for High Performance Applications, The University of Birmingham, for reading the manuscript of this paper.

References

1. R. C. GARVIE, R. H. J. HANNINK and R. T. PASCOE, *Nature (Lond.)* **258** (1975) 703.
2. G. K. BANSAL and A. H. HEUER, *J. Amer. Ceram. Soc.* **58** (1975) 235.
3. D. L. PORTER and A. H. HEUER, *ibid.* **60** (1977) 543.
4. N. CLAUSSEN, *ibid.* **59** (1976) 179.
5. *Idem, ibid.* **59** (1976) 49.
6. A. H. HEUER and L. W. HOBBS (eds), "Advances in Ceramics", Vol. 3, "Science and Technology of Zirconia I" (The American Ceramics Society, Columbus, OH 1981).
7. N. CLAUSSEN, M. RUHLE and A. H. HEUER (eds), "Advances in Ceramics", Vol. 12, "Science and Technology of Zirconia II" (The American Ceramics Society, Columbus, OH, 1984).
8. S. SOMIYA, N. YAMAMOTO and H. HANAGIDA (eds), "Advances in Ceramics", Vol. 24 (A and B) "Science and Technology of Zirconia III" (The American Ceramics Society, Westerville, OH, 1988).
9. K. TSUKUMA, K. UEDA and M. SHIMADA, *J. Amer. Ceram. Soc.* **68** (1985) C-4.
10. K. TSUKUMA and M. SHIMADA, *J. Mater. Sci. Lett.* **4** (1985) 857.
11. S. MERIANI and C. PALMONARI (eds), "Zirconia '88" (Elsevier Applied Science, London, 1989).
12. E. C. SUBBARAO, in "Advances in Ceramics", Vol. 3, "Science and Technology of Zirconia I", edited by A. H. Heuer and L. W. Hobbs (The American Ceramics Society, Columbus, OH, 1981) p. 1.
13. T. K. GUPTA, F. F. LANGE and J. H. BECHTOLD, *J. Mater. Sci.* **13** (1978) 1464.
14. G. M. WOLTEN, *Acta Crystall.* **17** (1964) 763.
15. C. T. LYNCH, in "High Temperature Oxides", Vol. 5-11, edited by A. M. Alper (Academic Press, New York, London, 1970) p. 193.
16. N. CLAUSSEN and M. RUHLE, in "Advances in Ceramics", Vol. 3, "Science and Technology of Zirconia I", edited by A. H. Heuer and L. W. Hobbs (The American Ceramics Society, Columbus, OH, 1981) p. 137.
17. N. CLAUSSEN, in "Advances in Ceramics", Vol. 12, "Science and Technology of Zirconia II", edited by N. Claussen, M. Ruhle and A. H. Heuer (The American Ceramics Society, Columbus, OH, 1984) p. 325.
18. R. W. RICE, B. A. BENDER, R. P. INGEL, T. W. COYLE and J. R. SPANN, in "Ultrastructure Processing of Ceramics, Glasses and Composites", edited by L. L. Hench and D. R. Ulrich (Wiley, New York, 1984) p. 507.
19. J. WANG and R. STEVENS, Final Report for BP, The University of Leeds (1990).
20. E. M. LARSEN, *J. Chem. Educ.* **10** (1951) 529.
21. W. FISCHER and W. CHALYBAEUS, *Z. Anorg. Chem.* **225** (1947) 79.
22. *Idem, ibid.* **225** (1947) 277.
23. H. A. ABODISHISH, US Pat. 4873 072 (10 October 1989).
24. I. ARSENIJE and I. LEUCA, *Rev. Roam. Chem.* **15** (1970) 1263.
25. N. CLAUSSEN, J. STEEB and R. F. PABST, *Amer. Ceram. Soc. Bull.* **55** (1977) 559.
26. G. V. HEVESEY, *Chem. Rev.* **2** (1925) 1.
27. T. MOELLER, "Inorganic Chemistry" (Wiley, New York, 1952).
28. C. PAULING, "The Nature of the Chemical Bond", 3rd Edn (Cornell Press, Ithaca, NY, 1960).
29. Powder Diffraction Files 6-318, 7-337, 8-342, 13-307, 14-534, 17-923, 21-904 and 24-1165, 1601 Park Lane, Swarthmore, PA 19081 (1976).
30. R. RUH, H. J. GARRETT, R. F. DOMAGALA and N. M. TALLEN, *J. Amer. Ceram. Soc.* **51** (1968) 23.
31. Y. SAKKA, Y. OISHI and K. ANDO, *J. Mater. Sci.* **17** (1982) 3101.
32. R. C. WEAST, "CRC Handbook for Chemistry and Physics", 65th Edn (CRC Press, Boca Raton, FL, 1985) p. 165.
33. R. D. SHANNON and C. T. PREWITT, *Acta Crystallogr.* **B25** (1969) 925.
34. E. J. LITTLE and M. M. JONES, *J. Chem. Educ.* **37** (1960) 231.
35. D. R. MARTIN and P. J. PIZZOLATO, in "Rare Metals Handbook", 2nd Edn, edited by C. A. Hampel (Reinhold, New York, 1954) p. 173.
36. B. MASON, "Principles of Geochemistry", Wiley, NY (1952).
37. P. GADSDEN, Mining Annual Report (1985) p. 112.
38. R. STEVENS, "An Introduction to Zirconia", 2nd Edn (Magnesium Electron, Twickenham, UK, 1986).
39. M. FLEISCHER, *Geol. Surv. Bull.* **1021A** (1955) 13.
40. Techn. Bull. (1985) Toya Soda Manufacturing Co. Ltd, 7-7, 1-Chome, Akasaka, Minato-Ku, Tokyo 107, Japan.
41. Techn. Bull. (1987) Nilcra Ceramics Ltd, 239 Separation Street, Northcote, Victoria, 3070, Australia.
42. L. L. FEHRENBACHER and L. A. JACOBSON, *J. Amer. Ceram. Soc.* **48** (1965) 157.
43. M. B. BEVER (ed) "Encyclopedia of Materials Science and Engineering" (Pergamon Press, Oxford, 1986) p. 2071.
44. A. C. RICHARDSON, D. W. SCOTT and J. F. SHEA, "Separation of Zirconium and Hafnium", Oak Ridge National Lab. Report No: AECD-2979 (1955).
45. R. F. DOMAGALA and R. RUH, *Amer. Soc. Matel Trans. Q* **58** (1965) 164.
46. Alfa Chemicals Catalog (1990).
47. Aldrich Chemicals Catalog (1990).
48. Techn. Bull. (1987) Teledyne Wah Chang Albany, Albany, OR, USA.
49. P. R. STASZAK, NASA Report: Nasa-cr-182800, Vol. 1 (1988).
50. C. A. SKIDMORE, Mining Annual Report (1991) p. 87.
51. F. FARNWORTH, S. L. JONES and I. McALPINE, in "Speciality Inorganic Chemicals", edited by R. Thompson (Royal Society of Chemistry, London, 1980) p. 249.
52. R. C. GARVIE, in "High Temperature Oxides Part II", edited by A. M. Alper (Academic Press, New York, 1970) p. 117.
53. E. S. GOULD, "Inorganic Reactions and Structures" (Holt, New York, 1955).
54. D. COSTER and G. HEVESEY, US Pat. 1 660 440 (1928).
55. V. YATIRAJAM, *J. Sci. Indust. Res.* **21D** (1962) 196.
56. J. A. MEGY and H. FREUND, *Metall. Trans.* **10B** (1979) 413.

57. E. M. LARSEN, p. 67 in "Inorganic Synthesis", edited by W. C. Fernelius and L. L. Quill, McGraw-Hill Book Co. Inc., NY (1950).
58. A. E. VAN ARKEL and J. H. DE BOER, *Z. Anorg. Allgem. Chem.* **141** (1924) 289.
59. W. C. SCHUMB and F. J. PITTMANN, *Anal. Chem.* **14** (1942) 512.
60. E. H. HUFFMAN and R. C. LILLY, *J. Amer. Chem. Soc.* **71** (1949) 4147.
61. Teledyne Industries Inc., US Pat. 1 539 958 (17 October 1975).
62. K. S. MAZDIYASNI, C. T. LYNCH and J. S. SMITH, *J. Amer. Ceram. Soc.* **48** (1965) 372.
63. K. S. MAZDIYASNI and L. M. BROWN, *ibid.* **53** (1970) 43.
64. K. S. MAZDIYASNI, C. T. LYNCH and J. S. SMITH, *ibid.* **50** (1967) 532.
65. L. M. BROWN and K. S. MAZDIYASNI, *ibid.* **53** (1970) 590.
66. S. L. DOLE, R. W. SCHEIDECKER, L. E. SHIERS, M. F. BERARD and O. HUNTER Jr, *Mater. Sci. Engng* **32** (1978) 277.
67. O. HUNTER Jr, R. W. SCHEIDECKER and S. TOJO, in "Materials Science Monograph 6", "Energy and Ceramics", edited by P. Vincenzini (Elsevier, New York, 1981) p. 879.
68. LI-MIN TAU, R. SRINIVASAN, R. J. DE ANGELIS, T. PINDER and B. H. DAVIS, *J. Mater. Res.* **3** (1988) 561.
69. R. SRINIVASAN and B. H. DAVIS, *J. Amer. Ceram. Soc.* **73** (1990) 1780.
70. H. TORAYA, M. YOSHIMURA and S. SOMIYA, *ibid.* **65** (1981) C-72.
71. *Idem, ibid.* **66** (1983) 148.
72. *Idem, ibid.* **66** (1983) 818.
73. *Idem*, in "Advances in Ceramics", Vol. 12, "Science and Technology of Zirconia II", edited by N. Claussen, M. Ruhle and A. H. Heuer (The American Ceramics Society, Columbus, OH, 1984) p. 806.
74. S. SOMIYA, M. YOSHIMURA, Z. NAKAI, K. HISHINUMA and T. KUMAKI, in "Advances in Ceramics", Vol. 21, "Ceramic Powder Science", edited by G. L. Messing, K. S. Mazdiyasi, J. W. McCauley and R. A. Harber (The American Ceramics Society, Westerville, OH, 1987) p. 43.
75. I. W. CHEN and Y. H. CHAIO, *Acta Metall.* **33** (1985) 1827.
76. *Idem*, in "Advances in Ceramics", Vol. 12, "Science and Technology of Zirconia II", edited by N. Claussen, M. Ruhle and A. H. Heuer (The American Ceramics Society, Columbus, OH, 1984) p. 33.
77. J. ADAM and M. D. ROGERS, *Acta Crystallogr.* **12** (1959) 951.
78. R. RUH and V. A. PATEL, *J. Amer. Ceram. Soc.* **56** (1973) 606.
79. R. E. HANN, P. R. SUITCH and J. L. PENTECOST, *ibid.* **68** (1985) C-285.
80. C. E. CURTIS, L. M. DONEY and J. R. JOHNSON, *ibid.* **37** (1954) 458.
81. D. W. STACY, J. K. JOHNSTONE and D. R. WILDER, *ibid.* **55** (1972) 482.
82. D. TAYLOR, *Br. Ceram. Trans. J.* **83** (1984) 32.
83. I. A. EL-SHANSHOURY, V. A. RUDENKO and I. A. IBRAHIM, *J. Amer. Ceram. Soc.* **53** (1970) 264.
84. V. B. GLUSHKOVA and M. V. KRAVCHINSKAYA, *Ceram. Intl.* **11** (1985) 56.
85. G. B. SENFT and V. S. STUBICAN, *Mater. Res. Bull.* **18** (1983) 1163.
86. J. D. BUCKLEY, PhD thesis, Iowa State University, Ames, IA (1967).
87. R. P. INGEL, D. LEWIS, B. A. BENDER and R. W. RICE, *Ceram. Eng. Sci. Proc.* **3** (1982) 577-86.
88. G. L. CLARK and D. H. REYNOLDS, *Ind. Engng Chem.* **29** (1937) 711.
89. J. D. McCULLOUGH and K. N. TRUEBLOOD, *Acta Crystallogr.* **12** (1959) 507.
90. D. K. SMITH and H. W. NEWKIRK, *ibid.* **18** (1965) 983.
91. G. TEUFER, *ibid.* **15** (1962) 1187.
92. G. K. BANSAL and A. H. HEUER, *Acta Metall.* **20** (1972) 1280.
93. R. RUH and W. R. CORFIELD, *J. Amer. Ceram. Soc.* **53** (1970) 126-129.
94. V. LANTERI, A. H. HEUER and T. E. MITCHELL, in "Advances in Ceramics", Vol. 12, "Science and Technology of Zirconia II", edited by N. Claussen, M. Ruhle and A. H. Heuer (The American Ceramics Society, Columbus, OH, 1984) p. 118.
95. E. K. KELLER (ed.), "Hafnium Dioxide and Its Compounds with Oxides of Rare Earth Elements" (Nauka, Leningrad, 1984).
96. A. G. BOGANOV, V. S. RUDENKO and L. P. MAKAROV, *Dokl. Acad. Nauk USSR* **160** (1965) 1065.
97. P. ALDEBERT, J. M. BADIE, J. P. TRAVERSE, J. L. BUEVOZ and G. ROULT, *Rev. Int. Hautes Temp. Refract.* **12** (1975) 307.
98. D. K. SMITH and C. F. CLINE, *J. Amer. Ceram. Soc.* **45** (1962) 249.
99. L. LIU, *Phys. Chem. Solids* **41** (1980) 331.
100. H. J. GARRETT, *Amer. Ceram. Soc. Bull.* **42** (1963) 201.
101. G. M. WOLTEN, *J. Amer. Ceram. Soc.* **46** (1963) 418.
102. A. H. HEUER and M. RUHLE, in "Advances in Ceramics", Vol. 12, "Science and Technology of Zirconia II", edited by N. Claussen, M. Ruhle and A. H. Heuer (The American Ceramics Society, Columbus, OH, 1984) p. 1.
103. J. E. BAILEY, *Proc. Roy. Soc. (Lond.)* **279A** (1964) 395.
104. C. F. GRAIN and W. J. CAMPBELL, *US Bur. Mines Rep. Invest.* 5982 (1982).
105. R. N. PATIL and E. C. SUBBARAO, *J. Appl. Crystallogr.* **2** (1969) 281.
106. S. K. FILATOV and V. A. FRANK-KAMENETSKII, *Sov. Phys. Crystallogr.* **14** (1969) 696.
107. R. C. GARVIE, *J. Phys. Chem.* **69** (1965) 1238.
108. *Idem, ibid.* **82** (1978) 218.
109. P. DURAN and C. PASCUAL, *J. Mater. Sci.* **19** (1984) 1178.
110. A. K. KUZNETSOV, *Zh. Neorg. Khim.* **20** (1975) 425.
111. M. V. KRAVCHINSKAYA, P. A. TIKHONOV and E. K. KOEHLER, *Ceram. Int.* **8** (1982) 70.
112. A. V. SHEVCHENKO, L. M. LOPATO, V. D. TKACHENKO and A. K. RUBAN, *IZV Akad. Nauk SSSR Neorg. Mater.* **23** (1987) 259.
113. V. B. GLUSHKOVA, L. V. SAZONOVA and F. GANIC, *ibid.* **14** (1978) 2096.
114. T. NOGUCHI and T. KOZUKA, *Sol. Energy* **10** (1966) 125.
115. P. CLAUSING, *Ceram. Abstr.* **11**(8) (1932) 471.
116. A. V. SHEVCHENKO, L. M. LOPATO, A. I. STEGNY, G. I. GERASIMYUK, V. S. DVERNYAKOV and V. V. PASICHNY, *Dokl. Akad. Nauk SSSR Ser. A8* (1979) 682.
117. T. YAMADA, M. YOSHIMURA and S. SOMIYA, *High Temp. High Press.* **18** (1986) 377.
118. T. YAMADA, M. MIZUNO and T. NOGUCHI, *Yogyo-Kyokai S57 Nenkai* (1982) 121.
119. R. W. SCHEIECKER, D. R. WILDER and H. MOELLER, *J. Amer. Ceram. Soc.* **60** (1977) 501.
120. A. V. SHEVCHENKO, L. M. LOPATO and A. K. RUBAN, *Dokl. Akad. Nauk SSSR Ser. B* **10** (1976) 925.
121. D. W. STACY, PhD thesis, Iowa University, Ames, IA (1971).
122. O. HUNTER Jr, R. W. SCHEIDECKER and S. TOJO, *Ceram. Int.* **5** (1979) 137.
123. J. E. BAILEY, D. LEWIS, Z. M. LIBRANT and L. J. PORTER, *Trans. J. Brit. Ceram. Soc.* **71** (1972) 25.
124. J. E. BAILEY, P. M. BILLS and D. LEWIS, *ibid.* **74** (1975) 247.
125. M. RUHLE and A. H. HEUER, in "Advances in Ceramics", Vol. 12, "Science and Technology of Zirconia II", edited by N. Claussen, M. Ruhle and A. H. Heuer (The American Ceramics Society, Columbus, OH, 1984) p. 14.
126. A. H. HEUER and M. RUHLE, *Acta Metall.* **33** (1985) 2101.
127. J. WANG, M. W. RAINFORTH and R. STEVENS, *Brit. Ceram. Trans. J.* **88** (1969) 1.
128. R. C. GARVIE and S. K. CHAN, *Physica* **150B** (1988) 203.
129. S. K. CHAN, in "Advances in Ceramics", Vol. 24, "Science and Technology of Zirconia III", edited by S. Somiya, N. Yamamoto and H. Hanagida (The American Ceramics Society, Westerville, OH, 1988) p. 983.
130. R. M. McMEEKING and A. G. EVANS, *J. Amer. Ceram. Soc.* **65** (1982) 242.

131. A. G. EVANS, in "Advances in Ceramics", Vol. 12, "Science and Technology of Zirconia II", edited by N. Claussen, M. Ruhle and A. H. Heuer (The American Ceramics Society, Columbus, OH, 1984) p. 193.
132. A. G. EVANS, in "Fracture in Ceramic Materials", edited by A. G. Evans (Noyes, New Jersey, 1985) p. 25.
133. F. F. LANGE, *J. Mater. Sci.* **17** (1982) 240.
134. D. L. PORTER and A. H. HEUER, *J. Amer. Ceram. Soc.* **60** (1977) 543.
135. R. H. J. HANNINK, *J. Mater. Sci.* **18** (1983) 457.
136. F. F. LANGE, *ibid.* **17** (1982) 225.
137. H. L. SCHICK, "Thermodynamics of Certain Refractory Compounds", Vol. 1 (Academic Press, New York, 1966).
138. E. D. WHITNEY, *J. Amer. Ceram. Soc.* **45** (1962) 612.
139. T. Y. TIEN, T. K. BROG and A. K. LI, *Int. J. High Tech. Ceram.* **2** (1986) 207.
140. T. K. BROG, PhD thesis, University of Michigan (1986).
141. G. BOCQUILLON, C. SUSSE and B. VODAR, *Rev. Hautes Temp. Refract.* **5** (1968) 249.
142. N. A. BENDELIANI, S. V. POPOVA and L. P. VERESCHAGIN, *Geochem. Int.* **4** (1967) 557.
143. G. BOCQUILLON and C. SUSSE, *Rev. Int. Hautes Temp. Refract.* **6** (1969) 263.
144. R. F. DOMAGALA and E. HECKENBACH, *Rev. Sci. Instrum.* **35** (1964) 1663.
145. N. A. BENDELIANI, S. V. POPOVA and L. F. VERESCHAGIN, *Geokhimiya* **6** (1967) 677.
146. R. SUYAMA, H. TAKUBO and S. KUME, *J. Amer. Ceram. Soc.* **68** (1985) C-237.
147. I. NETTLESHIP and R. STEVENS, *Int. J. High Tech. Ceram.* **3** (1987) 1.
148. V. B. GLUSHKOVA and M. V. KRAVCHINSKAYA, *Ceram. Int.* **11** (1985) 80.
149. V. S. STUBICAN, G. S. CORMAN, J. R. HELLMAN and G. SENFT, in "Advances in Ceramics", Vol. 12, "Science and Technology of Zirconia II", edited by N. Claussen, M. Ruhle and A. H. Heuer (The American Ceramics Society, Columbus, OH, 1984) p. 96.
150. E. RUDY and P. STECHER, *J. Less-Common Metals* **5** (1963) 78.
151. R. F. DOMAGALA and R. RUH, *ASM Trans. Q.* **62** (1969) 915.
152. R. RUH and H. J. GARRETT, *J. Amer. Ceram. Soc.* **50** (1967) 257.
153. C. DELAMARRE and M. PEREZ y JORBA, *Rev. Hautes Temp. Refract.* **2** (1965) 313.
154. J. G. ALLPRESS, H. J. ROSSELL and H. G. SCOTT, *Mater. Res. Bull.* **9** (1975) 455.
155. *Idem*, *J. Solid State Chem.* **14** (1975) 264.
156. J. G. ALLPRESS and H. J. ROSSELL, *ibid.* **15** (1976) 68.
157. C. DELAMARRE, *Rev. Int. Hautes Temp. Refract.* **9** (1972) 209.
158. A. K. KUZNETSOV, P. A. TIKHONOV and M. V. KRAVCHINSKAYA, *Zh. Neorg. Khim.* **20** (1975) 758.
159. L. M. LOPATO, A. V. SHEVCHENKO and E. I. ZOZ, *Izv. Akad. Khim.* **24** (1979) 2923.
160. F. GRAIN, *J. Am. Ceram. Soc.* **50** (1967) 288.
161. A. M. GAVRISH and E. I. ZOZ, *Izv. Akad. Nauk SSSR, Ser. Neorgan. Mater.* **14** (1978) 181.
162. V. S. STUBICAN, in "Advances in Ceramics", Vol. 24, "Science and Technology of Zirconia III", edited by S. Somiya, N. Yamamoto and H. Hanagida (The American Ceramics Society, Westerville, OH, 1988) p. 71.
163. M. G. SCOTT, *J. Mater. Sci.* **10** (1975) 1527-35.
164. R. M. CAILLET, C. H. DEPORTES, G. ROBERT and G. VITTE, *Rev. Int. Haut. Temp. Refract.* **4** (1967) 269.
165. M. DUCLOT, I. VICAT and C. H. DEPORTES, *J. Solid State Chem.* **2** (1970) 236.
166. M. PEREZ y JORBA, *Ann. Chim.* **7** (1962) 479.
167. A. ROUANET, *Compt. Rend. Acad. Sci. Paris* **267c** (1968) 1891.
168. G. S. CORMAN and V. S. STUBICAN, *Amer. Ceram. Soc.* **61** (1982) 337.
169. P. DURAN, in "Science of Ceramics", Vol. 10, edited by H. Hausner (Deutsche Keramische Gesellschaft, Koln, 1980) p. 209.
170. P. DURAN, *Ceram. Int.* **1** (1975) 10.
171. F. M. SPIRIDONOV and L. N. KOMISSAROVA, *Zh. Neorg. Khim.* **15** (1970) 875.
172. P. DURAN, *J. Amer. Ceram. Soc.* **60** (1977) 510.
173. M. R. THORNER, D. J. M. BEVAN and E. SUMMERVILLE, *J. Solid State Chem.* **2** (1970) 545.
174. P. DURAN, C. PASCUAL, J. P. COUTURES and S. R. SKAGGS, *J. Amer. Ceram. Soc.* **66** (1983) 101.
175. E. TANI, M. YOSHIMURA and S. SOMIYA, *ibid.* **66** (1983) 506.
176. A. M. GAVRISH, E. I. ZOZ, N. V. GUI'KO and A. E. SOLOV'EVA, *Izv. Akad. Nauk USSR Ser. Neorgan. Mater.* **11** (1975) 668.
177. F. M. SPIRIDONOV, LE. TKHYONG CHYONG and L. N. KOMISSAROVA, *Zh. Neorg. Khim.* **22** (1977) 588.
178. K. TSUKUMA and M. SHIMADA, *J. Mater. Sci.* **20** (1985) 1178.
179. H. F. SIMPSON, *Mater. Des. Eng.* **52** (1960) 16.
180. N. A. GODINA, E. K. KELER and V. S. RUDENKO, *J. Inorg. Chem.* **5** (1960) 1349.
181. A. HARARI, J. P. BOCQUET, M. HUBER and R. COLLONGUES, *C. R. Hebd. Seances Acad. Sci. Ser. C.* **267** (1968) 1316.
182. R. W. LYNCH and B. MOROSIN, *J. Amer. Ceram. Soc.* **55** (1972) 409.
183. K. S. MAZDIYASNI and L. M. BROWN, *ibid.* **53** (1970) 585.
184. R. G. HOLLENBERG, C. M. MARSCHALL, A. R. ROSENFELD, G. M. HOLLENBERG and R. RUH, *Mater. Sci. Engng* **15** (1974) 51.
185. G. A. CARLSON, J. L. ANDERSON, R. A. BRIESMEISTER, S. R. SKAGGS and R. RUH, *J. Amer. Ceram. Soc.* **60** (1977) 508.
186. R. RUH, G. M. HOLLENBERG, E. G. CHARLES and V. A. PATEL, *ibid.* **59** (1976) 495.
187. J. P. COUTURES and J. COUTURES, *ibid.* **70** (1987) 383.
188. L. F. CANADIEN, *High Temp. High Press.* **13** (1981) 97.
189. O. M. STANSFIELD, *J. Amer. Ceram. Soc.* **48** (1965) 436.
190. W. M. KRIVEN and E. BISCHOFF, in "Advances in Ceramics", Vol. 12, "Science and Technology of Zirconia II", edited by N. Claussen, M. Ruhle and A. H. Heuer (The American Ceramics Society, Columbus, OH, 1984) p. 425.
191. B. OHNYSTY and F. K. ROSE, *J. Amer. Ceram. Soc.* **47** (1964) 398.
192. M. F. TRUBELJA and V. S. STUBICAN, *ibid.* **71** (1988) 662.
193. N. CLAUSSEN, F. SIGULINSKI and M. RUHLE, in "Advances in Ceramics", Vol. 3, "Science and Technology of Zirconia I", edited by A. H. Heuer and L. A. Hobbs (The American Ceramics Society, Columbus, OH, 1981) p. 164.
194. B. V. BONDARENKO and B. M. TSAREV, *Radio. Elektron.* **4** (1959) 1059.
195. D. E. THOMAS and E. T. HAYES, "The Metallurgy of Titanium" (US Atomic Energy Commission, Washington, 1960).
196. R. J. ACKERMAN and R. J. THORN, in "Progress in Ceramics", edited by J. E. Burke (Pergamon Press, New York, 1961) p. 39.
197. R. W. SCHEIDECKER, *J. Mater. Sci.* **14** (1979) 2284.
198. S. L. DOLE, O. HUNTER Jr and F. W. CALDERWOOD, *J. Amer. Ceram. Soc.* **63** (1980) 136.
199. S. L. DOLE, O. HUNTER Jr and C. J. WOOGGE, *ibid.* **60** (1977) 488.
200. S. L. DOLE, MS Thesis Iowa State University, Ames, IA (1977).
201. R. RUH, G. W. HOLLENBERG, S. R. SKAGGS, S. D. STODDARD, F. D. GAC and E. G. CHARLES, *Amer. Ceram. Soc. Bull.* **60** (1981) 504.
202. S. R. SKAGGS, *Rev. Int. Hautes Temp. Refract.* **16** (1979) 157.
203. S. L. DOLE and O. HUNTER Jr, *J. Nucl. Mater.* **59** (1976) 207.
204. J. A. KUSZYK and R. C. BRADT, *J. Amer. Ceram. Soc.* **56** (1973) 420.
205. C. F. SMITH and W. B. CRANDALL, *ibid.* **47** (1964) 624.

206. R. M. SPRIGGS, *ibid.* **44** (1961) 628.
207. S. L. DOLE and O. HUNTER Jr, *ibid.* **66** (1983) C-47.
208. R. W. RICE, in "Properties and Microstructure", edited by R. K. MacCrone (Academic Press, New York, 1977) pp. 199-381.
209. C. D. WIRKUS and M. F. BERARD, *J. Mater. Sci.* **17** (1982) 109.
210. R. R. SUCHOMEL and O. HUNTER Jr, *J. Amer. Ceram. Soc.* **59** (1976) 149.
211. Y. IKUMA and A. V. VIRKAR, *J. Mater. Sci.* **19** (1984) 2233.
212. R. A. LANGE and B. OHNYSTY, see C. T. Lynch in [15].
213. N. CLAUSSEN, *Ber. Dtsch. Keram. Ges.* **54** (1977) 420.
214. J. WANG and R. STEVENS, *Ceram. Acta.* **3** (1991) 41.
215. F. F. LANGE and K. C. RADFORD, *J. Amer. Ceram. Soc.* **53** (1970) 420.
216. T. K. BROG, J. S. WALLACE and T. Y. TIEN, in "Fracture Mechanics of Ceramics", Vol. 8, edited by R. C. Bradt, A. G. Evans, D. P. H. Hasselman and F. F. Lange (Plenum, New York, 1986) p. 143.
217. H. W. CARPENTER, US Pat. 4 596 781 (1986).
218. E. K. STORMS, "The Refractory Carbides" (Academic Press, New York, 1967).
219. L. J. GAUCKLER, J. LORENZ, J. WEISS and G. PETZOW, in "Science of Ceramics", Vol. 10, edited by H. Hausner (Deut. Keram. Ges., 1980) p. 576.
220. E. D. WHITNEY, *J. Electrochem. Soc.* **112** (1965) 91.
221. J. K. JOHNSTONE, PhD thesis, Iowa University, Ames, IA (1970).
222. S. L. DOLE, O. HUNTER Jr, F. W. CALDERWOOD and D. J. BRAY, *J. Amer. Ceram. Soc.* **61** (1978) 486.

*Received 27 November
and accepted 12 December 1991*